



HAL
open science

Matrix Isolation Spectroscopy and Nuclear Spin Conversion of Propyne Suspended in Solid Parahydrogen

A. I. Strom, Alejandro Gutiérrez-Quintanilla, Michèle Chevalier, Justinas Ceponkus, Claudine Crépin, David T. Anderson

► **To cite this version:**

A. I. Strom, Alejandro Gutiérrez-Quintanilla, Michèle Chevalier, Justinas Ceponkus, Claudine Crépin, et al.. Matrix Isolation Spectroscopy and Nuclear Spin Conversion of Propyne Suspended in Solid Parahydrogen. *Journal of Physical Chemistry A*, 2020, 124 (22), pp.4471-4483. 10.1021/acs.jpca.0c02900 . hal-02944107

HAL Id: hal-02944107

<https://hal.science/hal-02944107>

Submitted on 22 Sep 2020

HAL is a multi-disciplinary open access archive for the deposit and dissemination of scientific research documents, whether they are published or not. The documents may come from teaching and research institutions in France or abroad, or from public or private research centers.

L'archive ouverte pluridisciplinaire **HAL**, est destinée au dépôt et à la diffusion de documents scientifiques de niveau recherche, publiés ou non, émanant des établissements d'enseignement et de recherche français ou étrangers, des laboratoires publics ou privés.

This document is confidential and is proprietary to the American Chemical Society and its authors. Do not copy or disclose without written permission. If you have received this item in error, notify the sender and delete all copies.

Matrix Isolation Spectroscopy and Nuclear Spin Conversion of Propyne Suspended in Solid Parahydrogen

| | |
|-------------------------------|--|
| Journal: | <i>The Journal of Physical Chemistry</i> |
| Manuscript ID | Draft |
| Manuscript Type: | Article |
| Date Submitted by the Author: | n/a |
| Complete List of Authors: | Strom, Aaron; University of Wyoming, Chemistry Gutierrez-Quintanilla, Alejandro; Aix-Marseille Université, Laboratoire PIIM, Team ASTRO Chevalier, Michele; Université Paris-Saclay Ceponkus, Justinas; Vilniaus Universitetas, Institute of Chemical Physics Crepin, Claudine; Institut des Sciences Moléculaires d'Orsay, Anderson, David; University of Wyoming, Department of Chemistry |
| | |

SCHOLARONE™
Manuscripts

Matrix Isolation Spectroscopy and Nuclear Spin Conversion of Propyne Suspended in Solid Parahydrogen

A. I. Strom,¹ A. Gutiérrez-Quintanilla,^{2,3a} M. Chevalier,² J. Ceponkus,⁴ C. Crépin,² and D. T. Anderson^{1b}

¹Department of Chemistry, University of Wyoming, Laramie, WY 82071-3838, USA

²Université Paris-Saclay, CNRS, Institut des Sciences Moléculaires d'Orsay, 91405, Orsay, France

³Instituto Superior de Tecnologías y Ciencias Aplicadas (InSTEC), Universidad de La Habana, Ave. Salvador Allende No. 1110, Quinta de los Molinos, La Habana 10400, Cuba

⁴Institute of Chemical Physics, Vilnius University, Sauletekio ave. 9 III, LT-10222 Vilnius, Lithuania

^aPresent address: Aix-Marseille Université, Laboratoire PIIM, Team ASTRO, Service 252, Saint Jérôme, Ave. Escadrille Normandie Niemen, 13013 Marseille, France.

^bAuthor to whom correspondence should be addressed: danderso@uwyo.edu

ABSTRACT: Parahydrogen (pH₂) quantum solids are excellent matrix isolation hosts for studying the rovibrational dynamics and nuclear spin conversion (NSC) kinetics of molecules containing indistinguishable nuclei with nonzero spin. The relatively slow NSC kinetics of propyne (CH₃CCH) isolated in solid pH₂ is employed as a tool to assign the rovibrational spectrum of propyne in the 600 – 7000 cm⁻¹ region. Detailed analyses of a variety of parallel ($\Delta K=0$) and perpendicular ($\Delta K=1$) bands of propyne indicate that the end-over-end rotation of propyne is quenched, but K rotation of the methyl group around the C_3 symmetry axis still persists. However, this single-axis K rotation is significantly hindered for propyne trapped in solid pH₂ such that the energies of the K rotational states do not obey simple energy level expressions. The NSC kinetics of propyne follows first-order reversible kinetics with a 287(7) min effective time constant at 1.7 K. Intensity-intensity correlation plots are used to determine the relative line strengths of individual *ortho*- and *para*-propyne rovibrational transitions, enabling an independent estimation of the ground vibrational state effective A'' constant of propyne.

1. Introduction

Spectroscopy of dopant molecules isolated in quantum condensed matter affords unique opportunities to probe the properties of weakly interacting, light mass media at the molecular level. In particular, inherently large amplitude dopant rotational motion is an incredibly useful probe of the quantum host dynamics determined by both kinetic and potential energy contributions, as one of the main qualifications of quantum condensed matter is the significance of the zero-point energy relative to the strength of the intermolecular forces.¹⁻⁴ Rovibrational spectroscopy of molecules and clusters embedded in ⁴He nanodroplets has long been used to probe the microscopic dynamics of this unique quantum fluid, where rotational fine structure is usually observed due to the Bose-Einstein statistics associated with ⁴He.⁵⁻⁹ The rovibrational spectra of dopants dissolved in liquid He nanodroplets are representative of the gas-phase molecular or cluster symmetry and yet the rotational constants are reduced compared to the isolated molecule. Solid parahydrogen (pH₂) provides another opportunity to study dopant rotation. However, stronger H₂-H₂ intermolecular forces relative to the intermolecular forces in He and the hexagonal close packed crystal structure in the solid pH₂ limit the propensity for observing dopant rotation in pH₂ matrices. Molecules that occupy single substitutional sites in the pH₂ crystal lattice (CH₄,¹⁰⁻¹³ NH₃,¹⁴ H₂O,^{15,16} HCl,¹⁷ and CO¹⁸ to name published examples) undergo nearly free rotation because the potential barriers to rotation are extremely small in this highly symmetric solvation environment. When bigger molecules are confined in solid pH₂ that occupy larger substitutional sites (double and larger), the end-over-end tumbling motions of the dopant are typically quenched.^{19,20} Yet molecules containing methyl rotors (CH₃) that behave as symmetric tops, such as CH₃F,²¹ or internal rotors, like CH₃OH,²² can continue to show spinning

1
2
3 motion of the CH₃ rotor. This spinning motion can be used to probe quantum solvation in larger,
4 more complex molecules, such as acetylacetone (CH₃(C=O)CH₂(C=O)CH₃).^{23,24}
5
6

7
8 The accessible temperature range is an important aspect of probing the rotational motions
9 of dopants trapped in quantum condensed matter. All of the molecules that demonstrate rotation
10 while solvated in solid pH₂ have small moments of inertia (CO being the only exception in the
11 literature¹⁸), and, thus, the rotational motion endures in spite of the rotational barriers induced by
12 the pH₂ host. This means that the energy of the lowest excited rotational state of the dopant is
13 also large with respect to the available thermal energy in the accessible temperature range in
14 solid pH₂ (1.5 to 4.3 K), so there is very little population in excited rotational levels that
15 significantly limits the number of rovibrational transitions that can be observed. Nonetheless,
16 closer examination of the list of rotating molecules reveals another important attribute, namely
17 indistinguishable hydrogen atoms. As a consequence of the symmetrization postulate of quantum
18 mechanics,²⁵ excited rotational states connected to the different nuclear spin isomers of the
19 dopant species can become kinetically trapped. Optimally, one would like to observe multiple
20 rovibrational transitions to help tease apart different rotational and vibrational contributions to
21 the measured transition energies in order to maximize the information content on the rotational
22 dynamics of the dopant isolated in solid pH₂. Of course, nuclear spin constraints are active for
23 methyl rotors in symmetric top molecules with two different moments of inertia, such as CH₃F.
24 In this case, sufficient population of excited $K=1$ rotational states are kinetically trapped, such
25 that transitions out of these levels are observable in the IR spectra of freshly deposited samples
26 of CH₃F isolated in solid pH₂.²¹ With time, these transitions out of excited rotational states
27 decrease in intensity due to condensed phase NSC. Thus, nuclear spin restrictions on the
28 rotational wavefunctions provide the means to study dopant rotational motion in low temperature
29
30
31
32
33
34
35
36
37
38
39
40
41
42
43
44
45
46
47
48
49
50
51
52
53
54
55
56
57
58
59
60

1
2
3 quantum hosts not possible in the fully equilibrated samples. This was successfully
4 demonstrated for CH_3F^{21} and $\text{CH}_3\text{OH}^{22}$ doped pH_2 solids.
5
6

7
8 Our groups, in Wyoming and Orsay, became interested in investigating the infrared
9 spectroscopy and solid state dynamics of methyl rotors trapped in solid pH_2 based on previous
10 experiments conducted in Orsay.^{23,24} Preliminary results on the infrared spectroscopy of propyne
11 in solid pH_2 , that are presented in the thesis of Gutiérrez,²⁶ were provided to the Wyoming group
12 to stimulate further collaborative studies. The idea is to develop useful spectroscopic tools to
13 gain information about how the quantum cavity around the methyl rotor perturbs the large
14 amplitude K rotational motion. Specifically, we want to develop analytical methods that employ
15 NSC phenomena to rigorously assign the measured infrared spectra for a number of molecular
16 dopants containing methyl groups. For example, which types of vibrational modes provide the
17 richest sources of information? If spectra contain significant fine structure, how can NSC be
18 used to assign the different peaks? A number of researchers have already addressed some of
19 these issues with much success,^{14,21-24,27} and we intend to refine the existing spectroscopic tools
20 to better determine how solvation in quantum condensed matter perturbs rotational dynamics in
21 dopant molecules. Furthermore, rovibrational spectroscopy can be used for NSC kinetics studies
22 of methyl rotor molecules with different attributes. Ultimately, our goal is to measure signatures
23 of NSC and quantitative nuclear spin populations of molecules for applications to photochemical
24 and reactive studies conducted in solid pH_2 .
25
26
27
28
29
30
31
32
33
34
35
36
37
38
39
40
41
42
43
44
45

46 **2. METHODS**

47
48
49 Most of the spectroscopic data presented here was acquired in the laboratory in Wyoming. Some
50 additional experiments were conducted in Orsay as this laboratory has the capability of
51 performing prolonged studies of a single pH_2 sample. A detailed description of the experimental
52
53
54
55
56
57
58
59
60

1
2
3 methods used in Orsay is published elsewhere,²⁸ and here we point out some important
4 differences between the two laboratories. In the laboratory in Orsay, samples are not obtained by
5 co-deposition but rather are deposited through a single deposition tube. The samples are thinner
6 and the concentration of dopant is higher than the samples grown in Wyoming. The lowest
7 temperature achieved in the laboratory in Orsay is 2.8 K, the highest resolution of the FTIR
8 spectrometer is 0.125 cm⁻¹, and samples can be kept frozen for several days at a time. As such,
9 the spectroscopic data from Orsay was recorded at 2.8 and 4.0 K, for samples that were kept
10 frozen for longer times and annealed, and thus could be used to complement and confirm the
11 results from the Wyoming laboratory.
12
13
14
15
16
17
18
19
20
21
22

23
24 The experimental apparatus for pH₂ matrix isolation spectroscopy in the Wyoming
25 laboratory has been discussed previously,^{14,29} so only details relevant to this study are presented
26 below. Propyne-doped pH₂ solids are grown via the rapid-vapor-deposition (RVD) technique
27 developed by Fajardo and Tam.^{30,31} This procedure involves the codeposition of independent pH₂
28 and propyne gas streams onto a precooled BaF₂ optical substrate held near ~2.5 K within a
29 sample-in-vacuum /He cryostat, producing millimeters-thick propyne-doped pH₂-enriched
30 samples in about ~30 mins. Enriched pH₂ gas (>99.97%) was rapidly introduced into the
31 cryostat via the outlet tube of a variable-temperature *ortho-to-para* (o/p) converter packed with
32 granular Fe(OH)₃ catalyst and backed by 800-1000 torr of normal H₂ gas (Linde, ≥99.999%)
33 passed through a needle-valve set to achieve flowrates of $\Phi_{H_2} = 200\text{-}500 \text{ mmol}\cdot\text{hr}^{-1}$. In this work,
34 the o/p converter is operated around 15 K producing pH₂ solids containing orthohydrogen (oH₂)
35 concentrations ≈100 ppm (approximated via gas-phase H₂ rotational partition functions or
36 determined experimentally using the oH₂-induced $Q_1(0)$ feature³¹ and sample thickness³²).
37
38
39
40
41
42
43
44
45
46
47
48
49
50
51
52
53
54
55
56
57
58
59
60

through a separate needle-valve set to achieve acceptable working concentrations that favor isolated monomers and disfavor propyne clusters. Exclusively as-deposited samples (hexagonal close packed (hcp) fractions between ≈ 50 -80%, estimated using the $U_1(0)$ feature²⁹) were studied in this work; annealing was conducted post-NSC to check for reversible and irreversible changes in measured IR spectra to confirm rovibrational assignments. Sample temperatures were measured using a pair of Si-diodes (attached to the OFHC Cu optical mount making thermal contact with the BaF₂ window) connected to a digital temperature controller. One diode (T_A) is located near to the cold finger of the cryostat, with the second (T_B) at the end of the optical holder; T_A is typically too cold to register temperatures (< 1.0 K), so sample temperatures are reported using $T_B \geq 1.5$ K. Temperatures are recorded autonomously (sampling rate of 1 Hz) using free chart recording software installed on the same computer used for spectroscopic measurements.

Total propyne monomer concentrations are measured via Beer's law, stated as²⁹

$$[\text{CH}_3\text{CCH}](\text{ppm}) = \frac{\ln(10) \int A_i(\tilde{\nu}) d\tilde{\nu}}{\epsilon_i^{p\text{H}_2} d} V_0 (1 \times 10^6), \quad (1)$$

where $A_i(\tilde{\nu}) = \log_{10} [I_0(\tilde{\nu})/I(\tilde{\nu})]$ is the decadic absorbance of the i^{th} vibrational mode of propyne integrated over the entire band area ($\tilde{\nu}$ to $\tilde{\nu} + d\tilde{\nu}$), $\epsilon_i^{p\text{H}_2} = 1.06 \epsilon_i^{\text{gas}}$ is the gas-phase integrated absorption coefficient corrected for the refractive index of solid $p\text{H}_2$,³² d is the thickness of the solid $p\text{H}_2$ slab,³² and $V_0 = 23.16(6) \text{ cm}^3 \text{ mol}^{-1}$ is the molar volume of solid $p\text{H}_2$ at /He temperatures.³³ Concentrations and $p\text{H}_2$ samples thicknesses are reported as weighted averages weighted by uncertainties. Integrated intensities from the literature and integration protocols are provided in the [Supporting Information](#), Table S2. Similarly, $p\text{H}_2$ sample thicknesses are reported as the weighted average of three independent measurements, integrated intensities of the $Q_1(0)+S_0(0)$, $S_1(0)+S_0(0)$ double transitions and $Q_R(0)$ IR absorptions bands³²

1
2
3 weighted by their absorption coefficients. Error propagation is performed in the usual way, in
4
5 which experimental as well as reported uncertainties in the literature are considered; typically,
6
7 the largest contribution to the stated errors stem from uncertainties in the integrated absorption
8
9 coefficients. A high-resolution FTIR spectrometer (Bruker IFS 120/5; $\Delta\tilde{\nu}=0.02\text{-}0.03\text{ cm}^{-1}$)
10
11 optimized for normal incidence transmission optical measurements was employed using
12
13 multiple optical setups: 1) a globar (GB; MIR) source, Ge coated KBr beamsplitter and N_2
14
15 cooled InSb detector, 2) a GB source, Ge coated KBr beamsplitter and N_2 cooled HgCdTe
16
17 (MCT) detector, 3) a tungsten filament (W; NIR) with a CaF_2 beamsplitter and 4) identical to
18
19 setup #2 with the addition of a long pass filter (LPF) with a 3861 cm^{-1} cutoff in the IR beam path
20
21 to eliminate absorptions by the $p\text{H}_2$ host. These optical setups were designed to record high-
22
23 fidelity IR spectra of specific vibrational modes of propyne located within the allowed
24
25 wavenumber ranges ($\Delta\tilde{\nu}=0.03\text{ cm}^{-1}$ over $600\text{-}4800\text{ cm}^{-1}$ for the MCT and $\Delta\tilde{\nu}=0.02\text{ cm}^{-1}$ over
26
27 $1800\text{-}5000\text{ cm}^{-1}$ or $1800\text{-}10,000\text{ cm}^{-1}$ for InSb with the Ge coated KBr or CaF_2 beamsplitters,
28
29 respectively). Furthermore, propyne concentrations deliberately span two orders of magnitude
30
31 (roughly 20-300 ppm) in order to enhance the sensitivity of target mode(s) in each experiment.
32
33
34
35
36
37

38 In order to study the NSC of propyne molecules isolated in solid $p\text{H}_2$ below He
39
40 temperatures, room temperature populations of excited rotational states of propyne must be
41
42 deposited into the solid much faster than they can relax, as in $\text{NH}_3/p\text{H}_2$ studies.¹⁴ Thus, the RVD
43
44 procedure was typically performed even more rapidly by setting $\Phi_{\text{H}_2}\approx 400\text{ mmol hr}^{-1}$ to enhance
45
46 observations of metastable propyne. Rapid-scan FTIR spectra recorded with modest time
47
48 resolution (3-5 min depending on averaging) were collected during the deposition step while
49
50 calibrating the dopant flowrate with Φ_{H_2} in order to enhance S/N and maximize contributions
51
52 from freshly-deposited rotating propyne molecules, and, of course, immediately post deposition
53
54
55
56
57
58
59
60

1
2
3 in order to monitor propyne NSC in as-deposited solid pH₂ samples near ~1.7 K until
4
5 equilibration. Equilibrium was achieved when intensity changes between difference spectra
6
7 were deemed undetectable, which was optimally on the order of the effective time constant of
8
9 propyne NSC, that is to say, relaxation periods of $\delta t \approx 300$ min or greater.

12 Important experimental parameters for each experiment in this study are summarized in
13
14 the [Supporting Information](#), Table S1, including optical setups, instrument resolution, H₂ flow
15
16 rates, pH₂ sample thicknesses, hcp fractions, propyne concentrations and the IR bands used to
17
18 determine them, and the duration of the relaxation period for each NSC kinetic run.

21 3. RESULTS AND DISCUSSION

24 Propyne (CH₃C≡CH) is the simplest linear hydrocarbon containing a methyl rotor. The gas-
25
26 phase spectroscopy of this prolate symmetric top ($A''=5.31$ cm⁻¹, $B''=0.29$ cm⁻¹)³⁴ has been
27
28 extensively studied as a model system to study vibrational energy flow in molecules.³⁴⁻³⁷
29
30 Belonging to the C_{3v} point group, propyne has ten fundamental vibrational modes with half of
31
32 the modes, $\nu_1 - \nu_5$, having A_1 symmetry, while the other half, $\nu_6 - \nu_{10}$, are degenerate with E
33
34 symmetry.^{38,39} Accordingly, parallel ($\Delta K=0$) and perpendicular transitions ($\Delta K=\pm 1$) of propyne
35
36 are expected for the A_1 and E symmetry vibrations, respectively. As discussed previously, the
37
38 end-over-end tumbling motion of propyne will likely be quenched similar to acetylene¹⁹ when
39
40 isolated in solid pH₂, but the spinning rotation of the methyl group, corresponding to the A
41
42 rotational constant, should continue to freely rotate similar to CH₃F.²¹ Based on van der Waals
43
44 radii and the structure of propyne,³⁴ propyne occupies a double substitution site in solid pH₂ with
45
46 cylindrical symmetry. Therefore, for propyne isolated in solid pH₂, we expect that the J and M_J
47
48 rotational quantum numbers appropriate for the gas-phase molecule in free space are lost, and
49
50 only the K rotational quantum number survives. Basically, the three-dimensional rotational
51
52
53
54
55
56
57
58
59
60

1
2
3 motion of propyne in free space transforms into one-dimensional rotation like a particle-on-a-
4 ring, and two angular librational degrees of freedom, upon suspension in the double substitution
5 site. Therefore, we break from using conventional gas-phase spectroscopic notation and instead
6 use a simplified notation, namely, $\Delta K_{\nu}(K'')$, where $\Delta K = -1, 0, +1$ are designated by P, Q, R and
7 ν' and K'' are the vibrational quanta in the upper state and the lower state K quantum number.
8
9

10
11 Each K rotational state is entangled with a single nuclear spin wavefunction of a specific
12 symmetry to satisfy the symmetrization postulate of quantum mechanics. For CH_3CCH with
13 three identical hydrogen nuclei (fermions), the *ortho* ($\Gamma_{ns}=A_1, I=3/2$) nuclear spin wavefunctions
14 combine with $K = 0, 3, 6, \dots$ rotational states in the ground vibrational state and *para* ($\Gamma_{ns}=E,$
15 $I=1/2$) nuclear spin wavefunctions combine with $K=1, 2, 4, 5, \dots$ rotational states. Thus, at the
16 high temperature limit ($T > 50$ K) a gaseous sample of propyne consists of roughly 50:50
17 mixtures of the *ortho* and *para* spin isomers because the factor of two greater nuclear spin weight
18 for the *ortho* spin isomer cancels the factor of two more $K \neq 3n$ rotational states of the *para*
19 isomer.
20
21

22
23 For A_1 symmetry vibrations, parallel transitions should lead to single peaks which
24 correspond to overlapping $Q_1(0)$ and $Q_1(1)$ transitions out of the lowest rotational states for the
25 *ortho* and *para* nuclear spin isomers, respectively. The fact that we observe $Q_1(0)$ transitions
26 (vide infra) is another observable in support of the fact that end-over-end rotation of propyne is
27 quenched; in the gas-phase no Q -branch is observed for the $K=0$ rotational sub-band.^{38,39} To the
28 extent that the A rotational constant is the same in the upper and lower vibrational states, these
29 transitions will overlap perfectly. However, if $A' - A'' \neq 0$, then the $Q_1(0)$ and $Q_1(1)$ transitions
30 will occur at slightly different wavenumbers ($Q_{\nu'}(1) - Q_{\nu'}(0) = A' - A''$) and there is a possibility
31 of resolving this K fine structure. In contrast, E type vibrations result in perpendicular bands
32
33
34
35
36
37
38
39
40
41
42
43
44
45
46
47
48
49
50
51
52
53
54
55
56
57
58
59
60

1
2
3 with well-resolved K sub-bands that correspond to the $R_1(0)$ transition for the *ortho* nuclear spin
4 modification and $P_1(1)$ and $R_1(1)$ transitions for the *para* nuclear spin isomer. For degenerate E
5 vibrations the vibrational angular momentum $l = \nu_i, \nu_i-2, \dots, -\nu_i$ in the upper state can align or
6 oppose the angular momentum of the K rotation.^{38,39} This gives rise to first-order Coriolis
7 splittings that can be modeled by the energy term $\pm 2(A\zeta)_v K l$, where ζ is the Coriolis coupling
8 constant. Given that the ground state A'' rotational constant is $\sim 5.31 \text{ cm}^{-1}$ for propyne in the gas-
9 phase,³⁴ at 1.7 K, transitions out of the $K'' = 2$ rotational state at approximately 21.2 cm^{-1} ought
10 to be extremely weak due to lack of population of this level. However, if the $K=2$ level is
11 significantly shifted to lower energies, then transitions out of this level may also be observed.
12
13
14
15
16
17
18
19
20
21
22
23

24 **3A. Infrared Spectroscopy of Propyne in Solid $p\text{H}_2$.** One of the main difficulties in
25 making detailed assignments of the infrared spectrum of propyne isolated in solid $p\text{H}_2$ is the fine
26 structure observed for some of the vibrational modes. This fine structure can be caused by
27 single-axis K rotation, but can also be due to a variety of causes, such as propyne- $(\text{oH}_2)_n$,
28 clusters, and one wants a way to selectively identify rovibrational transitions of freely rotating
29 propyne monomers. If the goodness of the K rotational quantum number is lost due to clustering
30 or trapping in defect sites, then we cannot differentiate between different nuclear spin isomers
31 using rovibrational spectroscopy. With this in mind, we begin with the assignment of the A_1
32 vibrational modes of propyne.
33
34
35
36
37
38
39
40
41
42
43
44

45 As discussed above, transitions involving A_1 vibrational modes should be observed as
46 single peaks (or two overlapping peaks) close to the gas-phase vibrational origins. Typically,
47 $p\text{H}_2$ matrix shifts¹⁻⁴ are less than 1% and, thus, for well-resolved single peaks, vibrational
48 assignments are made simply by comparing the measured peak wavenumber with a potential
49 gas-phase origin. Shown in Figure 1(a) are absorption spectra from 750 to 1500 cm^{-1} for a 2.5(2)
50
51
52
53
54
55
56
57
58
59
60

1
2
3 mm thick, 200(39) ppm propyne/pH₂ sample recorded at 1.70(1) K at 2.63 (red) and 491 min
4
5 (blue) after deposition. The spectra are intentionally offset from zero to show the difference
6
7 spectrum. All the A_1 vibrational modes in this region are easily assigned via comparison with the
8
9 vibrational origins reported in the literature and these A_1 vibrational assignments are presented in
10
11 Table 1. However, by constructing difference spectra recorded at short and long time delays
12
13 after deposition, we can try to resolve these two bands based on NSC. RVD of room
14
15 temperature propyne into solid pH₂ at 1.7 K kinetically traps the higher energy *para* nuclear spin
16
17 isomer in the $K = 1$ rotational state due to slow NSC relative to vibrational and rotational
18
19 relaxation. Assuming that NSC is slow albeit measurable, then by constructing difference
20
21 spectra⁴⁰ as $(A_t - A_\infty)$ as a function of time ($t = 0$ defined as the end of deposition) allows us to
22
23 identify absorptions due to the *ortho* and *para* nuclear spin isomers of propyne. On the basis of
24
25 the +/- phase of the peak in the difference spectrum, positive peaks are due to the *para* spin
26
27 isomer and will be maximum at $t=0$ and must decrease with time. Negative peaks are minimum
28
29 at $t=0$ and increase to a maximum at $t = \infty$ (*i.e.*, ≈ 4 h) as population is transferred to the lower
30
31 energy $K=0$ rotational state of the *ortho* nuclear spin isomer. Furthermore, peaks in the
32
33 difference spectra can be used to selectively identify absorptions due to propyne monomers that
34
35 are undergoing unhindered K rotation. As we will show, some peaks in the absorption spectra do
36
37 not appear in the difference spectra and this obviously inhibits the *para* and *ortho* assignments of
38
39 these peaks. Nevertheless, peaks with sufficient intensity in the difference spectra, that exhibit
40
41 quantitatively the correct NSC kinetics, allow the nuclear spin isomer responsible for that
42
43 transition to be rigorously assigned.
44
45
46
47
48
49

50
51 Careful inspection of the difference spectrum shown in Figure 1(b) illustrates our strategy
52
53 for making detailed assignments. For A_1 symmetry parallel bands ($\Delta K=0$), the wavenumber
54
55
56
57
58
59
60

1
2
3 difference in the $Q_1(0)$ and $Q_1(1)$ sub-bands must be comparable to the FWHM of the individual
4 absorptions to detect a difference signal. All the A_1 vibrational bands shown in Figure 1(a) do
5 not show strong difference signals. Based on gas phase measurements,^{41,42} detecting difference
6 signals for both the ν_5 and ν_4 fundamentals should be difficult because the $A' - A''$ differences are
7 small, -0.0073 cm^{-1} and 0.017 cm^{-1} , respectively, and both peaks have modest integrated
8 intensities (see [Supporting Information](#), Table S2). Obviously, small population differences are
9 detected with higher sensitivity using absorptions with large integrated intensities. The $2\nu_9^0$
10 overtone peak at 1254.47 cm^{-1} has a large integrated intensity⁴³ ($16.81(29) \text{ km mol}^{-1}$), but again
11 based on gas phase measurements⁴⁴ the $A' - A'' = -0.00292 \text{ cm}^{-1}$ value is quite small. The small
12 difference signal for the $2\nu_9^0$ overtone peak shown in Figure 1(b) therefore shows that the $Q_2(0)$
13 and $Q_2(1)$ absorption features are strongly overlapped making it difficult to determine the
14 splitting. Thus, all the A_1 vibrational modes displayed in Figure 1 do not show a clear difference
15 spectrum and are assigned to overlapping $Q_1(0)/Q_1(1)$ peaks. However, as we will show for ν_2 ,
16 when the $A' - A''$ difference becomes a little larger, a clear difference signal can be measured for
17 A_1 type vibrations that provide information on the vibrational origin and the value of $A' - A''$ for a
18 particular vibrational mode.

19
20
21
22
23
24
25
26
27
28
29
30
31
32
33
34
35
36
37
38
39
40
41 For E -type vibrational symmetry modes that produce perpendicular bands ($\Delta K = \pm 1$), the
42 rovibrational transitions for the *para* and *ortho* spin isomers are spectrally resolved making
43 assignments rather straightforward. For example, also shown in Figure 1 is the ν_7 (see
44 [Supporting Information](#), Figure S5) absorption of propyne near 1450 cm^{-1} . This mode shows a
45 number of peaks in absorption, but the difference spectrum reveals a positive peak at 1443.54
46 cm^{-1} and a negative peak at 1455.12 cm^{-1} for the *para* and *ortho* nuclear spin isomers,
47 respectively. These nuclear spin assignments are rigorous, and we can therefore tentatively
48
49
50
51
52
53
54
55
56
57
58
59
60

1
2
3 assign these two peaks to the $P_1(1)$ and $R_1(0)$ transitions of the *para* and *ortho* nuclear spin
4 isomers, respectively. The energy difference between these two transitions predicted using the
5 gas-phase rotational constants⁴¹ (neglecting centrifugal distortion) is 14.45 cm^{-1} , which compares
6 favorably to the measured value of 11.58 cm^{-1} and is also consistent with assigning the higher
7 wavenumber transition to the *ortho* nuclear spin isomer, as indicated by the difference spectrum.
8 Similarly, the ν_8 mode shows (see inset in Figure 1b) positive and negative difference spectra
9 peaks that are assigned to the *para* $P_1(1)$ and *ortho* $R_1(0)$ peaks, respectively. These two
10 rovibrational transitions are typically the strongest for *E*-type vibrational modes and the $R_1(1)$
11 transition is also observed sometimes, but is usually much broader and harder to detect. The
12 rovibrational assignments of *E* type vibrational bands are also listed in Table 1. In what follows,
13 we examine various propyne bands in greater detail in order to articulate some of the challenges
14 associated with making detailed rovibrational assignments.

15
16
17
18
19
20
21
22
23
24
25
26
27
28
29
30
31 After assigning *ortho* and *para* nuclear spin symmetries to the various peaks present in
32 the spectrum of propyne using the difference spectra, we can attempt K rotational assignments
33 using conventional energy levels expressions developed for gas-phase prolate symmetric
34 tops.^{38,39} However, since we expect that J is no longer a good quantum number, the energy level
35 expressions are modified to consider only terms associated with single-axis K rotation
36 (neglecting centrifugal distortion). In the [Supporting Information](#), Section 2 various expressions
37 are discussed for Q , R , and P transitions with $K'' = 0, 1, \text{ and } 2$ for both parallel (A_1) and
38 perpendicular (E) rovibrational bands. This information is used to compare the measured
39 transition wavenumbers of propyne with gas-phase results to attempt detailed assignments.

40
41
42
43
44
45
46
47
48
49
50
51
52 The first band investigated in detail was the ν_2 (symmetric methyl CH stretch)
53 fundamental near 2941 cm^{-1} . This vibrational mode has a large integrated band strength (see
54
55
56
57
58
59
60

1
2
3 [Supporting Information](#), Table S2) and therefore is sensitive to small population differences. As
4
5 we will show, this band can be used to effectively measure the NSC kinetics of propyne in solid
6
7 pH_2 . The ν_2 spectrum recorded at 0.02 cm^{-1} resolution is shown in Figure 2. Spectra recorded
8
9
10 5.08 and 291.8 min after deposition are shown in Figure 2(a) as red and blue traces, respectively.
11
12 Both spectra are intentionally offset from zero to better show the resulting difference spectrum.
13
14 Shown in Figure 2(b), therefore, is the difference spectrum. The difference spectrum displays
15
16 the signature lineshape for overlapping $Q_1(1)$ and $Q_1(0)$ transitions for the two nuclear spin
17
18 isomers, namely, the positive $Q_1(1)$ peak is assigned to the *para* isomer and the negative $Q_1(0)$
19
20 peak to the *ortho* isomer. Based on the gas-phase rotational constants,^{35,45} these two transitions
21
22 are predicted³⁵ to be split by 0.055 cm^{-1} (or 0.090 based on Ref. 45) with the $Q_1(0)$ transition of
23
24 the *ortho* nuclear spin isomer at higher wavenumbers. For propyne isolated in solid pH_2 , we
25
26 observe these two bands with the same energetic ordering as measured in the gas-phase, and with
27
28 a splitting of around 0.11 cm^{-1} . These measurements demonstrate that the change in the A
29
30 rotational constant upon ν_2 excitation is very small, but does not provide information on the
31
32 value of A in either the ground or excited vibrational states. It also demonstrates how the
33
34 difference spectrum of a parallel band can be used to measure the growth and decay in the
35
36 populations of the two nuclear spin isomers of propyne. By definition, the difference spectrum is
37
38 only sensitive to propyne populations that undergo K -rotation and NSC and therefore rejects
39
40 overlapping propyne features that do not contribute to NSC. For example, careful examination
41
42 of Figure 2 reveals that the total ν_2 lineshape is not well represented by the sum of two
43
44 overlapping pseudo-Voigt peaks, but rather this absorption has a shoulder to the low
45
46 wavenumber side ($\sim 2934.4 \text{ cm}^{-1}$) that does not change in intensity with time. In addition,
47
48 integration of the entire difference spectrum results in a value of zero indicating that the line
49
50
51
52
53
54
55
56
57
58
59
60

1
2
3 strengths for the two transitions are approximately equal. This is consistent with both these
4
5 transitions being pure vibrational transitions (not rovibrational) and the $Q_1(0)$ transition has the
6
7 same integrated band strength as the $Q_1(1)$ peak. This is a direct ramification of the loss of J as a
8
9 good quantum number such that the $Q_1(0)$ transition is possible for the matrix isolated propyne.

10
11
12 In Figure 3, we present the full spectrum of ν_6 (antisymmetric methyl CH stretch) which
13
14 is representative of a perpendicular band.^{35,46} Here we see more deviations from gas-phase
15
16 behavior, signaling perturbations in the K rotational motion. For the absorption spectra recorded
17
18 at short and long times after deposition, we measure approximately 7 peaks excluding the two
19
20 very weak peaks at the extremes of the spectral range displayed in Figure 3. However, in the
21
22 difference spectrum, three peaks are absent (marked with asterisks in Fig. 3) and we only have
23
24 clear difference signals for four peaks, indicating that the three central peaks shown in Figure 3
25
26 do not show the same NSC kinetics as the others. It is possible that these peaks are due to
27
28 propyne-(oH₂)_n clusters that form irreversibly due to the stronger attractive intermolecular forces
29
30 between propyne and oH₂ compared to pH₂; however, assignment of these cluster peaks extends
31
32 beyond the scope of this work. Based on the idea that the strongest transitions should be out of
33
34 the $K = 0$ and 1 rotational states, we should observe one $R_1(0)$ peak for the *ortho* nuclear spin
35
36 isomer, and two transitions for the *para* isomer, namely, $P_1(1)$ and $R_1(1)$. We do observe two
37
38 peaks for the *para* spin isomer, but we also observe two $R_1(0)$ peaks for the *ortho* spin isomer.

39
40
41 As first demonstrated by Lee, Wu and Hougen,²¹ we can attempt to make K rotational
42
43 assignments of the ν_6 band based on a simple energy level expression for single-axis K rotation
44
45 and the molecular constants measured in the gas-phase (see [Supporting Information](#), Section 2).
46
47 To begin, we make the simplifying assumption that we can use the average of the two observed
48
49 $R_1(0)$ transitions for the $R_1(0)$ transition wavenumber ($R_1(0)_{\text{avg}} \approx 2979.7 \pm 0.7 \text{ cm}^{-1}$). As we will
50
51
52
53
54
55
56
57
58
59
60

1
2
3 show, it doesn't matter how we treat this obvious deviation from gas-phase behavior, we cannot
4 extract a consistent set of molecular constants. We first assigned the three rovibrational
5 transitions shown in Fig. 3 corresponding to $K'' = 0, 1$ and assuming the gas-phase Coriolis
6 constant ($\zeta_6=0.07250$)⁴⁶ is preserved, we determined the three molecular constants presented in
7 Table 2. This gave reasonable results consistent with reduced A constants for propyne K -rotation
8 in solid $p\text{H}_2$. However, next, we used all 5 rovibrational transitions labeled in Figure 3
9 corresponding to $K'' = 0, 1, 2$. Whereas the assignment of $K''=2$ transitions seems beyond a
10 doubt, by comparison with gas phase values (Table 1), the relation $R_1(2) - P_1(2) = 2[R_1(1) -$
11 $P_1(1)]$, deduced from the simplified model, is not fulfilled, independent of the value of the
12 Coriolis constant. All variations of the fitting procedure given in the [Supporting Information](#),
13 Section 2, fixed and floated ζ_6 , and including a D_K distortion constant resulted in fits that could
14 not reproduce the transition wavenumbers to within experimental precision (e.g., $rms = 1.2 \text{ cm}^{-1}$).
15 This is clearly a statement that the measured spectra, assigned via the methods described, do not
16 readily conform to expressions determined for single-axis K rotation. Thus, comparison of the
17 determined molecular constants with gas-phase values to make detailed K rotational assignments
18 is likely misleading, especially when assumptions must be made given a limited number of
19 transitions. This is an intrinsic problem with conducting these types of rovibrational assignments
20 that only involve a few transitions and therefore lack built-in redundancies in the spectrum (such
21 as four line combination differences), there is no way to rigorously test potential assignments.
22 Surely, qualitative insights can be ascertained, but true predictive understanding of the energy
23 patterns can only be advanced by comparing with fully quantum mechanical simulations that
24 include interactions of the dopant with the surrounding $p\text{H}_2$ solid.
25
26
27
28
29
30
31
32
33
34
35
36
37
38
39
40
41
42
43
44
45
46
47
48
49
50
51
52
53
54
55
56
57
58
59
60

1
2
3 The *E* type ν_7 (CH_3 skeletal deformation) vibrational mode at roughly 1450 cm^{-1} , shown
4
5 previously in Figure 1, was also studied in detail (see [Supporting Information](#), Figure S5 for the
6
7 expanded spectrum). For this band, we only observed the $P_1(1)$, $R_1(0)$, and $R_1(1)$ transitions and,
8
9 thus, to extract molecular constants from this mode we had to assume that the gas-phase Coriolis
10
11 coupling constant ($\zeta_7 = -0.31424$)⁴¹ is largely unchanged upon solvation in solid pH_2 . Similar to
12
13 the ν_6 band, the $R_1(0)$ peak consists of two partially resolved peaks and therefore we used the
14
15 average peak position ($R_1(0)_{\text{AVG}} = 1454.9\text{ cm}^{-1}$). There is some doubt in the assignment of the
16
17 $R_1(1)$ transition, either to a feature at 1458.4 or 1473.88 cm^{-1} . However, using either $R_1(1)$
18
19 assignment, the simplified model with the gas phase Coriolis coupling constant leads to
20
21 unphysical A rotational constants, and importantly, to a different A'' constant than the ν_6 analysis.
22
23 The three molecular constants determined from this analysis with $R_1(1)$ at 1473.88 cm^{-1} are
24
25 presented in Table 2. Once again, this analysis demonstrates that quantitative analysis of the
26
27 extracted molecular constants from K -rotational assignments of only three transitions is
28
29 potentially misleading. The only other *E* type vibration where this analysis is possible is the
30
31 $\nu_3+\nu_8$ combination band and the results are also presented in Table 2. Clearly, the analysis of
32
33 each band leads to a different A'' constant each time. The fact that this type of analysis does not
34
35 produce a consistent ground state A'' constant implies that either the assumption that the Coriolis
36
37 constant does not change, or the assumed energy level expression, is incorrect. Applying a
38
39 similar type of analysis to the three *E*-type rovibrational bands reported in the literature²¹ for
40
41 CH_3F in solid pH_2 leads to a similar conclusion; each band produces a different ground state A''
42
43 rotational constant. This suggests that the K -rotational energy levels of both methyl rotor
44
45 molecules, CH_3CCH and CH_3F , are not well described by simple single-axis K rotational energy
46
47 level expression.
48
49
50
51
52
53
54
55
56
57
58
59
60

1
2
3 We repeatedly observed two $R(0)$ lines for many of the E -type propyne bands ($\nu_6, \nu_7, \nu_8,$
4 $2\nu_6$). This is most likely due to the selection rules for C_{3v} symmetric tops, the fact that Coriolis
5 perturbations are possible in upper degenerate vibrational states, and the loss of the J quantum
6 number for propyne isolated in solid pH_2 . Neither of the rotational levels connected by the $P_1(1)$
7 rovibrational transition are effected by Coriolis perturbations and the $R_1(1)$ line connects E
8 symmetry rotational levels.⁴⁷ But the $R_1(0)$ transition accesses the $K=1$ rotational state in the
9 upper vibrational state and thus in the gas-phase accesses alternating A_1 and A_2 rotational states
10 as a function of J . In the present case where the J quantum number is lost, Coriolis perturbations
11 of the upper rotational state could produce two spectrally resolved $R_1(0)$ transitions.
12 Furthermore, observation of two $R_1(0)$ transitions also contributes to the difficulty of extracting
13 consistent molecular constants from the analysis of the $P_1(1)$, $R_1(0)$, and $R_1(1)$ transitions. Thus,
14 it appears that the vibrational angular momentum generated in the upper degenerate vibrational
15 state that is coupled to the K -rotation produces shifts in the transition wavenumbers on the order
16 of the K sub-band spacing. Two $R_1(0)$ transitions could also appear when considering a removal
17 of the degeneracy of the upper E vibrational state due to the solid environment. If the
18 perturbation due to the solid environment is large enough to induce torsional barriers, the $K'' = 0$
19 and 1 levels are better represented by A and E levels, respectively, in the periodic torsional
20 potential (splitting due to H atom tunneling) as was described in Ref. 23 in the case of the
21 acetylacetone molecule. The analysis of the NSC process remains the same, but the structure
22 presented in the spectrum by the $P_1(1)$ and especially the $R_1(1)$ transitions is difficult to assign.

23
24
25
26
27
28
29
30
31
32
33
34
35
36
37
38
39
40
41
42
43
44
45
46
47
48
49
50
51
52
53
54
55
56
57
58
59
60
These same types of discrepancies are not found in the interpretation of rovibrational
spectra of molecules isolated in superfluid He nanodroplets.⁵⁻⁹ Typically, the measured
rotational constants for molecules dissolved in He nanodroplets are reduced (39% and 95% for

1
2
3 heavy and light rotors) from gas-phase values, and distortion constants can be anomalously large,
4
5 but the standard spectroscopic signatures are preserved along with the selection rules based on
6
7 the symmetry of the gas-phase transition dipole moment.⁵⁻⁹ For example, the parallel ($\Delta K=0$) ν_1
8
9 spectrum (acetylenic C-H stretch) of propyne was recently revisited for propyne isolated in He
10
11 nanodroplets.^{48,49} The spectrum displays *P*, *Q*, and *R* branches appropriate for a C_{3v} symmetric
12
13 top molecule. Comparison between the fitted constants for gas-phase propyne and propyne
14
15 solvated in He nanodroplets shows that the *B* rotational constant is reduced to 26.0(1)% and
16
17 25.6(1)% of its gas-phase value for the ground and $\nu=1$ excited vibrational states, respectively,
18
19 and the Δ_J distortion constant increases by a factor of 5100 compared to the gas-phase.
20
21 However, using these effective rotational constants, the spectrum is relatively well reproduced
22
23 demonstrating that the selection rules are preserved.⁴⁹ Note that the ν_1 band is a parallel band so
24
25 that the spectrum is not sensitive to the *A* constant directly, but rather the difference in *A*
26
27 constants with vibrational excitation. Unfortunately, the corresponding ν_1 spectrum for propyne
28
29 isolated in solid pH_2 is not very informative because the difference spectrum shows multiple
30
31 positive and negative peaks (see [Supporting Information](#), Figure S6). Nonetheless, it is clear that
32
33 isolation of propyne in solid pH_2 perturbs the rotational motion in a qualitatively different way;
34
35 there is no end-over-end rotation in solid pH_2 while in liquid 4He the end-over-end rotational
36
37 motion is preserved (although greatly hindered) and so are the selection rules. This means that
38
39 the rovibrational dynamics of molecules in solid pH_2 are more difficult to assign rigorously and
40
41 therefore also harder to interpret. While both He and pH_2 are quantum hosts, one is a liquid and
42
43 the other a solid and this leads to very different rotational dynamics of guest molecules. In solid
44
45 pH_2 , the rotational dynamics are significantly perturbed, end-over-end rotational is quenched,
46
47 and the selection rules are altered (no *Q*-branch for $K=0$ in the gas-phase), such that the observed
48
49
50
51
52
53
54
55
56
57
58
59
60

1
2
3 infrared spectra of molecular dopants isolated in solid pH₂ exhibiting *K*-axis rotation are not so
4 easily assigned via comparison to gas-phase spectra. However, the spectra assigned via the
5 methods used here provide new data sets that can be modeled using quantum mechanical
6 dynamic calculations to learn more about the pH₂ cage dynamics.
7
8
9
10

11
12 **3B. Nuclear Spin Conversion Kinetics.** We initiate our analysis of the NSC kinetics of
13 propyne in solid pH₂ using the ν_2 vibrational band near 2935 cm⁻¹. As described above, since ν_2
14 is a parallel band, peaks associated with separate *ortho* and *para* nuclear spin isomers are not
15 observed directly. Therefore, difference spectra recorded at various times after deposition are
16 utilized to measure the effective rate constant for *para-to-ortho* NSC of propyne. As described
17 in detail in the [Supporting Information](#), Section 1, each difference spectrum is fit to a sum of two
18 normalized symmetric pseudo-Voigt profiles⁵⁰ in order to quantify time-dependent intensity
19 changes in the two overlapping absorptions that are resolved in the difference spectrum. The two
20 difference peaks in Figure 2 can be assigned to the *para* ($K=1, I=1/2$) and *ortho* ($K=0, I=3/2$)
21 nuclear spin isomers. A representative difference spectrum for ν_2 fit to the sum of two pseudo-
22 Voigt lineshape functions is shown in Figure 4; the difference spectrum is well modeled by this
23 functional form allowing a number of parameters to be extracted from each spectral trace (see
24 [Supporting Information](#), Section 1 for more details). The strength of this procedure is that the
25 peak areas of components in an overlapping band, which are conserved quantities, are extracted
26 directly from the analysis in order to study their temporal behavior. It turns out that the time
27 dependence of the two components in the ν_2 difference spectra are well-fit to solutions of first-
28 order kinetics equations, where the effective lifetime of propyne NSC, τ_{eff} , is statistically
29 equivalent for both components to within the standard errors of the fitted parameters (see
30 [Supporting Information](#), Table S4).
31
32
33
34
35
36
37
38
39
40
41
42
43
44
45
46
47
48
49
50
51
52
53
54
55
56
57
58
59
60

Representative kinetic traces for the ν_2 (A_1) vibrational mode of propyne are shown in Figure 5a. As described earlier, the red and blue data points represent the *para* and *ortho* peak areas determined from fits to the difference spectra. The lines represent the results of least-squares fits of the data to first-order kinetics equations (see below). Note that the way we calculate the difference spectra means that both peak areas should decay to zero as the propyne nuclear spin populations come into equilibrium at long times after deposition. For the data shown in Figure 5a, we did not wait long enough to achieve equilibrium as evidenced by the crossing of the fits above and below zero. However, this does not affect the determined τ_{eff} time constant due to the nature of first-order kinetics. Individual time constants are determined for each peak and are well matched. Repetition of this analysis in four separate experiments yields highly reproducible results (see [Supporting Information](#), Table S4). Examination of Figure 5a also shows that the two peak areas are symmetrically displaced around zero indicating that the line strengths associated with these two peaks are comparable, although the peak FWHM's differ (see Fig. 2).

The ν_6 and ν_7 perpendicular bands were also analyzed to determine effective NSC time constants for propyne. To quantify the NSC kinetics, the ν_6 and ν_7 bands are broken into segments; fortunately, there is enough separation between the various peaks to integrate the peaks corresponding to *ortho* ($R_1(0)$) and *para* ($P_1(1)$ and $R_1(1)$) nuclear spin isomer populations. The integrated intensities are well-fit to first-order kinetic equations given by

$$I_{para}(t) = I_{para}(\infty) + (I_{para}(0) - I_{para}(\infty))\exp(-t/\tau) \quad (2)$$

$$I_{ortho}(t) = I_{ortho}(0) + (I_{ortho}(\infty) - I_{ortho}(0))[1 - \exp(-t/\tau)] \quad (3)$$

in which the fitted lifetimes agree statistically with the ν_2 data to within error ([Supporting Information](#), Table S4). Representative kinetic traces for ν_6 and ν_7 are shown in Figure 5b and

1
2
3 5c, respectively. The kinetic traces in Fig. 5b and 5c are different from 5a because they were
4 constructed from the integration of absorption spectra, not difference spectra. We did check that
5 the total integrated intensity of each band remains constant over the time window of the kinetic
6 analysis. Eleven separate kinetic analyses of the ν_2 , ν_6 and ν_7 bands of propyne all agree with
7 each other and produce a weighted average time constant of $\tau_{eff} = 287(7)$ min.
8
9

10
11
12
13
14
15 As a further test of this kinetic analysis, we also fitted the difference spectrum of the ν_2
16 mode of $^{13}\text{CH}_3^{12}\text{C}_2\text{H}$ present in natural abundance ($\sim 1.1\%$) for the experiment with the highest
17 propyne concentration. The other ^{13}C isotopologs likely overlap with the ν_2 mode of the most
18 abundant isotopolog.^{35,51} As expected, this peak was also well-fit by expressions (Eq. 2 and 3)
19 and gave a time constant of $\tau_{eff} = 170(20)$ min, which is approximately 1.7(3) times faster than
20 the value determined for the $^{12}\text{C}_3\text{H}_4$ isotopomer. The reason for the faster NSC in $^{13}\text{CH}_3^{12}\text{C}_2\text{H}$ is
21 likely because the $^{13}\text{C}(I=1/2)$ nucleus interacts with the H-atoms on the methyl group via
22 magnetic dipole-dipole coupling which introduces an additional relaxation channel not open to
23 the normal isotopolog.⁵²⁻⁵⁴ It would be interesting to put the ^{13}C on the acetylenic carbons to see
24 if the time constant increases for the more remote atom with non-zero nuclear spin.
25
26
27
28
29
30
31
32
33
34
35
36
37

38 **3C. Measuring the *para-to-ortho* ratio for propyne in solid pH_2 at low temperature.**

39
40 The thermodynamic equilibrium concentrations for the *para* and *ortho* nuclear spin isomers of
41 propyne are given by the respective rotational partition functions as a function of temperature.
42 This *para-to-ortho* ratio (*POR*) is defined here as the equilibrium constant for the reversible,
43 first-order nuclear spin conversion process between the two spin isomers of propyne, namely,
44
45
46
47
48
49

$$50 \text{ortho-propyne} \leftrightarrow \text{para-propyne}; \text{POR} = \frac{[\text{para}]}{[\text{ortho}]} \quad (4)$$

51
52
53 As discussed earlier, in the high temperature limit the *POR* approaches unity, whereas this ratio
54 goes to zero at $T \rightarrow 0$ K. We were therefore interested in calculating the experimental *POR*
55
56
57
58
59
60

1
2
3 measured in these studies after the system has come into equilibrium as another way to
4 determine the energy splitting between the $K=1$ and $K=0$ rotational states. However, in order to
5 do this necessitates that we transform our integrated intensities into relative populations, which
6 means the line strengths of individual rovibrational transitions must be determined. In
7 calculating propyne concentrations using Eq. (1) we simply integrate over the entire band and
8 use the integrated IR band intensities given in the [Supporting Information](#), Table S2, but if we
9 want rotational populations we must deal with rovibrational line strengths. To do this rigorously
10 is difficult, thus, we used an approximation that has been used by others,⁵⁵ where we assume that
11 the populations in the $K=0$ and $K=1$ follow this equation, $n_{K=1} + n_{K=0} = 1$, that is, that the system
12 is well described as a two component system, then the relative line strengths can be determined
13 from intensity-intensity correlation plots.⁵⁵ Correlation plots of the intensities for various
14 transitions in ν_6 can be generated as shown in the [Supporting Information](#), Figure S9 and Table
15 S5. Furthermore, this approach allows us to estimate the *POR* as a function of time during an
16 experiment and also to estimate the energy of the $K=1$ excited rotational state of the *para* nuclear
17 spin isomer.

18
19
20
21
22
23
24
25
26
27
28
29
30
31
32
33
34
35
36
37
38 We analyzed the ν_6 spectra for six different experiments in terms of the *POR* to see if
39 general trends could be quantified. A representative *POR* trace is shown in Figure 6. As stated
40 earlier, the high temperature statistical limit is $POR = 1.0$, where there is an equal mixture of
41 *ortho* and *para* nuclear spin isomers. Upon RVD of room temperature propyne gas into solid
42 pH_2 , the initial $POR \approx 0.9$ at ~ 2.5 K during deposition. By the end of deposition ($t=0$), the *POR*
43 drops to a value of ~ 0.75 and after deposition it continues to decay at 1.7 K. From a fit to the
44 experimental data, the *POR* decays to an equilibrium value of ~ 0.17 . This is an order of
45 magnitude greater than the theoretical limit predicted using the gas-phase rotational energies at
46
47
48
49
50
51
52
53
54
55
56
57
58
59
60

1
2
3 equilibrium at 1.7 K ($POR = 0.0117$) and therefore signals a lowering of the $K=1$ level. We note
4
5 that this analysis does suffer from potential systematic errors due to contributions of the non-
6
7 rotating propyne absorption at 2978.29 cm^{-1} to the integrated intensity of the $R_1(0)$ peak, the fact
8
9 that there are two $R_1(0)$ peaks for ν_6 , and errors in the measured temperature. However, given
10
11 the difficulties in determining A'' spectroscopically, this might be the best way to measure the
12
13 ground state $K=1$ and $K=0$ energy splitting.
14
15

16
17 Using this approach, we estimate the energy difference between the lowest *para* ($K=1$)
18
19 and *ortho* ($K=0$) rotational states, or in other words the effective A'' constant. This analysis
20
21 predicts a value of $2.2(6)\text{ cm}^{-1}$ and is compared with the spectroscopic constants in Table 2. This
22
23 value suggests that propyne K -rotation is strongly perturbed. This analysis predicts that the A''
24
25 rotational constant is about 42% of the gas-phase value and therefore the population of the *para*
26
27 nuclear spin isomer at equilibrium at 1.7 K is significantly greater than what is predicted using
28
29 the gas-phase rotational constants. Given that we measure an equilibrium POR value of ~ 0.15 at
30
31 1.7 K, the approximate temperature where all the experiments were conducted, this implies that
32
33 the elementary rate constants for the reversible first-order NSC kinetics are significantly different
34
35 from the measured effective rate constant.⁵⁶ We can use the measured k_{eff} and $POR(1.7(1)\text{ K},$
36
37 $t=\infty)$ for five experiments (Expt. 3 was discarded) to determine $k_{p \rightarrow o} = 3.00(9) \times 10^{-3}\text{ min}^{-1}$ and
38
39 $k_{o \rightarrow p} = 4.4(11) \times 10^{-4}\text{ min}^{-1}$.
40
41
42
43
44

45 Another way therefore to refine the POR determination would be to perform kinetic
46
47 experiments at different temperatures. We should be able to measure different asymptotic values
48
49 of POR (at equilibrium) as a function of temperature. All the experiments in the Wyoming
50
51 laboratory were conducted at the deposition temperature because we did not want to complicate
52
53 the analysis of the difference spectra by including changes due to annealing or oH_2 diffusion,
54
55
56
57
58
59
60

1
2
3 which can occur over comparable timescales relative to NSC at elevated temperatures.¹⁻⁴
4
5 However, the group in Orsay conducted experiments for samples that were equilibrated for
6
7 longer times at 2.8 K, and were annealed at 4.0 K for brief periods of time. The group in Orsay
8
9 uses a closed-cycle cryostat and thus is capable of monitoring the same sample for days. The
10
11 group in Wyoming uses a bath cryostat and thus can only hold samples for approximately 10
12
13 hours without the need to refill with liquid helium. Spectra from the Orsay laboratory were
14
15 analyzed using the same procedure and line strengths determined in Wyoming. The measured
16
17 values from the two laboratories are presented in Figure 7. The lines presented in Figure 7
18
19 represent *PORs* calculated for single-axis *K*-rotation ($E = A''K^2$) with effective A'' constants equal
20
21 to 1.00 cm⁻¹, 2.22 cm⁻¹, and 5.31 cm⁻¹, respectively. Error bars on each measurement are
22
23 calculated using propagation of errors. The data from the two labs are somewhat consistent with
24
25 greater *PORs* calculated at higher temperatures in Orsay. All the data lies between the two
26
27 limiting values of $A'' = 1.00$ and 5.31 cm⁻¹. As can be seen in Figure 7, there is significant scatter
28
29 in the measured *PORs*, but the level of agreement is promising given the difficulties in making
30
31 intensity based measurements. We hope this work motivates similar measurements for different
32
33 methyl rotor molecules and we want to continue to refine these measurements for propyne by
34
35 conducting further experiments in both laboratories.
36
37
38
39
40
41

42 It is interesting to compare the NSC rate constant determined here for propyne with the
43
44 one measured at 3.3 K for CH₃F isolated in solid pH₂.²¹ At 3.3 K, based on our analysis of
45
46 propyne with $A''=2.2(6)$ cm⁻¹, we would predict a *POR* of approximately 0.3 which would imply
47
48 $k_{eff}(3.3 \text{ K}) \approx 3.8 \times 10^{-3} \text{ min}^{-1}$ as compared to $2.2(5) \times 10^{-3} \text{ min}^{-1}$ for the fast NSC rate constant
49
50 measured over the first 5 hours for CH₃F solvated in solid pH₂ at 3.3 K.²¹ Previous
51
52 measurements of CH₃F NSC found bi-exponential behavior that the authors ascribed to fast oH₂
53
54
55
56
57
58
59
60

1
2
3 assisted NSC of CH₃F, followed by slower ($k = 3.7(8) \times 10^{-4} \text{ min}^{-1}$) NSC when the oH₂
4
5 concentration drops below a critical value.²¹ There is no evidence for bi-exponential behavior in
6
7 the current NSC kinetics, but measurements over larger time windows would be helpful.
8
9 Interestingly, the opposite behavior was found for NSC of ClCH₂ trapped in solid pH₂ where the
10
11 conversion rate decreased by a factor of 1.5 for samples with 10% oH₂.²⁷ All the measurements
12
13 conducted in Wyoming were only performed for up to 8 hours. Preliminary results on longer
14
15 timescales performed in Orsay show the time evolution of the three peaks marked with an
16
17 asterisk in Figure 3 (and Figures S4 and S5), and at much longer timescales, two peaks decrease
18
19 with time and one increases, meaning that the behavior at long times is more complex. An
20
21 analysis of these peaks in terms of oH₂ clustering or different matrix sites must be performed to
22
23 go further in this analysis.
24
25
26
27
28
29

30 31 4. CONCLUSIONS

32
33 We present here a detailed spectroscopic analysis of propyne isolated in solid pH₂. This analysis
34
35 shows how NSC can be used to rigorously assign the nuclear spin isomer responsible for a given
36
37 rovibrational transition, provided that the molecules exhibit single-axis K rotational motion.
38
39 Further, through the analysis of three separate perpendicular rovibrational bands, a detailed K
40
41 rotational assignment is not possible that delivers a consistent set of ground state rotational
42
43 constants. This demonstrates that the rotational levels of propyne solvated in solid pH₂ are not
44
45 well described by simple one-dimensional free rotor expressions, and that quantum calculations
46
47 that include intermolecular interactions with the quantum host are likely necessary for acceptable
48
49 agreement with experiment. This data therefore contains detailed experimental information on
50
51 how the quantum cavity influences the large amplitude rotational motion of a dopant, but the
52
53
54
55
56
57
58
59
60

1
2
3 complication of how best to extract this information still remains. It is hoped that the procedures
4
5 used in this study are applicable to a wide variety of molecules containing methyl rotors to
6
7 permit systematic studies.
8
9

10 The NSC kinetics of propyne in solid pH₂ show single-exponential decay indicative of a
11
12 reversible first-order process. Careful analysis of three separate bands all lead to an average
13
14 effective time constant of $\tau_{eff} = 287(7)$ min for NSC at 1.7 K. This time constant is comparable
15
16 to the fast time constant extracted for CH₃F suspended in solid pH₂, but as discussed in the
17
18 previous section, the NSC of propyne should be measured over longer time periods to see if it
19
20 too shows bi-exponential behavior similar to CH₃F. Using intensity-intensity correlation plots,
21
22 we are able to determine the relative line strengths of different propyne rovibrational transitions
23
24 that allow the *POR* to be calculated. This data suggests that using the RVD technique we are
25
26 able to trap ~75% of the higher rotational energy *para* nuclear spin isomer immediately post
27
28 deposition. Further, by measuring the *POR* after full thermal equilibration, analysis from both
29
30 labs suggests that the *A''* rotational constant is significantly reduced from its gas phase value. A
31
32 reduction in the *A''* rotational constant would be suspected for a hindered rotor in solid pH₂ and
33
34 thus further experiments could better determine this value and hopefully bring the predicted *A''*
35
36 values estimated from spectroscopic measurements in the two laboratories into better agreement.
37
38 We plan to study NSC in a series of molecules containing methyl groups in order to see if trends
39
40 emerge and to further develop these analytical tools and procedures by testing them on a variety
41
42 of molecules.
43
44
45
46
47
48

49 ACKNOWLEDGEMENTS

50
51 This work was sponsored in part by the Chemistry Division of the US National Science
52
53 Foundation (CHE 13-62497). AIS is grateful to the UW Department of Chemistry for providing
54
55
56
57
58

1
2
3 a Summer Research Fellowship during his first summer of graduate school when some of this
4
5 work was conducted. The Orsay group acknowledges the RTRA Triangle de la Physique (2013-
6
7 0436T REACMAQ) for support and the French-Lithuanian PHC GILIBERT program (42125XF
8
9 and S-LZ-19-1 from RCL).
10
11
12
13
14
15
16
17
18
19
20
21
22
23
24
25
26
27
28
29
30
31
32
33
34
35
36
37
38
39
40
41
42
43
44
45
46
47
48
49
50
51
52
53
54
55
56
57
58
59
60

REFERENCES

- (1) Bahou, M.; Das, P.; Lee, Y.-F.; Wu, Y.-J.; Lee, Y.-P. Infrared spectra of free radicals and protonated species produced in para-hydrogen matrices. *Phys. Chem. Chem. Phys.* **2013**, *16*, 2200-2210.
- (2) Momose, T.; Fushitani, M.; Hoshina, H. Chemical reactions in quantum crystals. *Int. Rev. Phys. Chem.* **2005**, *24*, 533-552.
- (3) Oka, T. High-Resolution Spectroscopy of Solid Hydrogen. *Annu. Rev. Phys. Chem.* **1993**, *44*, 299-333.
- (4) Yoshioka, K.; Raston, P. L.; Anderson, D. T. Infrared spectroscopy of chemically doped solid parahydrogen. *Int. Rev. Phys. Chem.* **2006**, *25*, 469-496.
- (5) Callegari, C.; Conjusteau, A.; Reinhard, I.; Lehmann, K. K.; Scoles, G. Superfluid hydrodynamic model for the enhanced moments of inertia of molecules in ^4He . *Phys. Rev. Lett.* **1999**, *83*, 5058-5061.
- (6) Callegari, C.; Lehmann, K. K.; Schmied, R.; Scoles, G. Helium nanodroplet isolation rovibrational spectroscopy: Methods and recent results. *J. Chem. Phys.* **2001**, *115*, 10090-10110.
- (7) Grebenev, S.; Toennies, J. P.; Vilesov, A. F. Superfluidity within a small helium-4 cluster: The microscopic Andronikashvili experiment. *Science* **1998**, *279*, 2083-2086.
- (8) Hartmann, M.; Miller, R. E.; Toennies, J. P.; Vilesov, A. F. High-resolution molecular spectroscopy of van der waals clusters in liquid helium droplets. *Science* **1996**, *272*, 1631-1634.
- (9) Toennies, J. P.; Vilesov, A. F. Superfluid helium droplets: A uniquely cold nanomatrix for molecules and molecular complexes. *Angew. Chem. Int. Ed.* **2004**, *43*, 2622-2648.
- (10) Miki, M.; Momose, T. Rovibrational transitions and nuclear spin conversion of methane in parahydrogen crystals. *Low Temp. Phys.* **2000**, *26*, 661-668.
- (11) Miyamoto, Y.; Fushitani, M.; Ando, D.; Momose, T. Nuclear spin conversion of methane in solid parahydrogen. *J. Chem. Phys.* **2008**, *128*, 114502-1-10.
- (12) Momose, T. Rovibrational states of a tetrahedral molecule in a hexagonal close-packed crystal. *J. Chem. Phys.* **1997**, *107*, 7695-7706.
- (13) Tam, S.; Fajardo, M. E.; Katsuki, H.; Hoshina, H.; Wakabayashi, T.; Momose, T. High resolution infrared absorption spectra of methane molecules isolated in solid parahydrogen matrices. *J. Chem. Phys.* **1999**, *111*, 4191-4198.
- (14) Ruzi, M.; Anderson, D. T. Matrix isolation spectroscopy and nuclear spin conversion of NH_3 and ND_3 in solid parahydrogen. *J. Phys. Chem. A* **2013**, *117*, 9712-9724.
- (15) Fajardo, M. E.; Lindsay, C. M. Crystal field splitting of rovibrational transitions of water monomers isolated in solid parahydrogen. *J. Chem. Phys.* **2008**, *128*, 014505-1-4.
- (16) Fajardo, M. E.; Tam, S.; DeRose, M. E. Matrix isolation spectroscopy of H_2O , D_2O , and HDO in solid parahydrogen. *J. Mol. Struct.* **2004**, *685-696*, 111-127.

- 1
2
3 (17) Anderson, D. T.; Hinde, R. J.; Tam, S.; Fajardo, M. E. High-resolution spectroscopy of
4 HCl and DCl isolated in solid parahydrogen: Direct, induced, and cooperative infrared
5 transitions in a molecular quantum solid. *J. Chem. Phys.* **2002**, *116*, 594-607.
6
7 (18) Fajardo, M. E.; Lindsay, C. M.; Momose, T. Crystal field theory analysis of rovibrational
8 Spectra of carbon monoxide monomers isolated in solid parahydrogen. *J. Chem. Phys.*
9 **2009**, *130*, 244508-1-10.
10
11 (19) Lee, Y.-C.; Venkatesan, V.; Lee, Y.-P.; Macko, P.; Didiriche, K.; Herman, M. Infrared
12 spectra of C₂H₂ under jet-cooled and para-H₂ matrix conditions. *Chem. Phys. Lett.* **2007**,
13 *435*, 247-251.
14
15 (20) Tam, S.; Fajardo, M. E. Observation of the high-resolution infrared absorption spectrum
16 of CO₂ molecules isolated in solid parahydrogen. *Low Temp. Phys.* **2000**, *26*, 653-660.
17
18 (21) Lee, Y.-P.; Wu, Y.-J.; Hougen, J. T. Direct spectral evidence of single-axis rotation and
19 ortho-hydrogen-assisted nuclear spin conversion of in solid parahydrogen. *J. Chem. Phys.*
20 **2008**, *129*, 104502-1-6.
21
22 (22) Lee, Y.-P.; Wu, Y.-J.; Lees, R. M.; Xu, L.-H.; Hougen, J. T. Internal rotation and spin
23 conversion of CH₃OH in solid para-hydrogen. *Science* **2006**, *311*, 365-368.
24
25 (23) Lozada-Garcia, R. R.; Ceponkus, J.; Chevalier, M.; Chin, W.; Mestdagh, J.-M.; Crépin,
26 C. Nuclear spin conversion to probe the methyl rotation effect on hydrogen-bond and
27 vibrational dynamics. *Angew. Chem. Int. Ed.* **2012**, *51*, 6947-6950.
28
29 (24) Gutierrez-Quintanilla, A.; Chevalier, M.; Ceponkus, J.; Lozada-Garcia, R. R.; Mestdagh,
30 J.-M.; Crepin, C. Large amplitude motions within molecules trapped in solid
31 parahydrogen. *Faraday Discuss.* **2018**, *212*, 499-515.
32
33 (25) Pauli, W. The connection between spin and statistics. *Phys. Rev.* **1940**, *58*, 716-722.
34
35 (26) Gutierrez-Quintanilla, A. Molecules and complexes with hydrogen bond: solvation and
36 photoreactivity in cryogenic matrices. Ph.D., Universite Paris-Saclay, 2016.
37
38 (27) Miyamoto, Y.; Tsubouchi, M.; Momose, T. Infrared spectroscopy of chloromethyl radical
39 in solid parahydrogen and its nuclear spin conversion. *J. Chem. Phys.* **2013**, *117*, 9510-
40 9517.
41
42 (28) Gutierrez-Quintanilla, A.; Chevalier, M.; Platakyte, R.; Ceponkus, J.; Rojas-Lorenzo, G.
43 A.; Crepin, C. 2-Chloromalonaldehyde, a model system of resonance-assisted hydrogen
44 bonding: vibrational investigation. *Phys. Chem. Chem. Phys.* **2018**, *20*, 12888-12897.
45
46 (29) Strom, A. I.; Fillmore, K. L.; Anderson, D. T. Hydrogen atom catalyzed ortho-to-para
47 conversion in solid molecular hydrogen. *Low Temp. Phys.* **2019**, *45*, 676-688.
48
49 (30) Fajardo, M. E.; Tam, S. Rapid vapor deposition of millimeters thick optically transparent
50 parahydrogen solids for matrix isolation spectroscopy. *J. Chem. Phys.* **1998**, *108*, 4237-
51 4241.
52
53 (31) Tam, S.; Fajardo, M. E. Ortho/para hydrogen converter for rapid deposition matrix
54 isolation spectroscopy. *Rev. Sci. Instrum.* **1999**, *70*, 1926-1932.
55
56 (32) Fajardo, M. E. Solid parahydrogen thickness revisited. *Appl. Spectrosc.* **2019**, *73*, 1403-
57 1408.
58
59
60

- 1
2
3 (33) Silvera, I. F. The solid molecular hydrogens in the condensed phase - Fundamentals and
4 static properties. *Rev. Mod. Phys.* **1980**, *52*, 393-452.
5
6 (34) El Idrissi, M. I.; Lievin, J.; Herman, M.; Campargue, A.; Graner, G. The vibrational
7 energy pattern in propyne ($^{12}\text{CH}_3^{12}\text{C}_2\text{H}$). *Chem. Phys.* **2001**, *265*, 273-289.
8
9 (35) McIlroy, A.; Nesbitt, D. J. High-resolution, slit jet infrared spectroscopy of
10 hydrocarbons: Quantum state specific mode mixing in CH stretch-excited propyne. *J.*
11 *Chem. Phys.* **1989**, *91*, 104-113.
12
13 (36) McIlroy, A.; Nesbitt, D. J.; Kerstel, E. R. T.; Pate, B. H.; Lehmann, K. K.; Scoles, G.
14 Sub-Doppler, infrared laser spectroscopy of the propyne $2\nu_1$ band: Evidence of z-axis
15 Coriolis dominated intramolecular state mixing in the acetylenic CH stretch overtone. *J.*
16 *Chem. Phys.* **1994**, *100*, 2596-2611.
17
18 (37) Portnov, A.; Blockstein, L.; Bar, I. Vibrational structure and methyl C–H dynamics in
19 propyne. *J. Chem. Phys.* **2006**, *124*, 164301-164301-164308.
20
21 (38) Herzberg, G.: *Molecular Spectra and Molecular Structure - Infrared and Raman Spectra*
22 *of Polyatomic Molecules*; Krieger Publishing Company: Malabar, Florida, 1988; Vol.
23 Vol. II.
24
25 (39) Hollas, J. M.: *High Resolution Spectroscopy*; 2nd ed.; John Wiley & Sons, Ltd.: New
26 York, New York, 1998.
27
28 (40) Szczepanski, J.; Ekern, S.; Vala, M. Spectroscopy and photochemistry of the $\text{C}_3\cdot\text{H}_2\text{O}$
29 complex in argon matrices. *J. Phys. Chem.* **1995**, *99*, 8002-8012.
30
31 (41) Henfrey, N. F.; Thrush, B. A. A high-resolution study of the ν_7 band of propyne. *J. Mol.*
32 *Spectrosc.* **1985**, *113*, 426-450.
33
34 (42) Pracna, P.; Muller, H. S. P.; Urban, S.; Horneman, V.-M.; Klee, S. Interactions between
35 vibrational polyads of propyne, $\text{H}_3\text{CC}\equiv\text{CH}$: Rotational and rovibrational spectroscopy of
36 the levels around 1000 cm^{-1} . *J. Mol. Spectrosc.* **2009**, *256*, 152-162.
37
38 (43) Es-Sebbar, E.; Jolly, A.; Benilan, Y.; Farooq, A. Quantitative mid-infrared spectra of
39 allene and propyne from room to high temperatures. *J. Mol. Spectrosc.* **2014**, *305*, 10-16.
40
41 (44) Henfrey, N. F.; Thrush, B. A. A high-resolution study of the $2\nu_9$ band of propyne. *J. Mol.*
42 *Spectrosc.* **1987**, *121*, 139-149.
43
44 (45) Xing, X.; Reed, B.; Lau, K.-C.; Baek, S.-J.; Bahng, M.-K.; Ng, C. Y. Assignment of
45 rovibrational transitions of propyne in the region of $2934\text{-}2952\text{ cm}^{-1}$ measured by two-
46 color IR–vacuum ultraviolet laser photoion-photoelectron methods. *J. Chem. Phys.* **2007**,
47 *127*, 044313-1-5.
48
49 (46) Go, J.; Cronin, T. J.; Perry, D. S. A free-jet infrared double resonance study of the
50 threshold region of IVR. The ν_6 , $\nu_1+\nu_6$, and $2\nu_1$ bands of propyne. *Chem. Phys.* **1993**,
51 *175*, 127-145.
52
53 (47) Zhao, D.; Linnartz, H. The high-resolution infrared spectrum of the $\nu_3 + \nu_8$ combination
54 band of jet-cooled propyne. *Chem. Phys. Lett.* **2014**, *595-596*, 256-259.
55
56 (48) Nauta, K.; Miller, R. E.: In *Atomic and Molecular Beams, the State of the Art*;
57 Camparque, R., Ed.; Springer-Verlag: Berlin, 2001; pp 775-792.
58
59
60

- 1
2
3 (49) Gutierrez-Quintanilla, A.; Briant, M.; Mengesha, E.; Gaveau, M. A.; Mestdagh, J. M.;
4 Soep, B.; Crepin, C.; Poisson, L. A Helium NanoDroplet Isolation (HENDI)
5 investigation of the weak hydrogen bonding in the propyne dimer (CH₃CCH)₂. *Phys.*
6 *Chem. Chem. Phys.* **2018**, *20*, 28658-28666.
- 8 (50) Stancik, A. L.; Brauns, E. B. A simple asymmetric lineshape for fitting infrared
9 absorption spectra. *Vib. Spectrosc.* **2008**, *47*, 66-69.
- 11 (51) Doney, K. D.; Zhao, D.; Linnartz, H. High-resolution infrared spectra of the ν_1
12 fundamental bands of mono-substituted ¹³C propyne isotopologues. *J. Phys. Chem. A*
13 **2018**, *122*, 582-589.
- 15 (52) Nagels, B.; Bakker, P.; Hermans, L. J. F.; Chapovsky, P. L. Nuclear spin conversion in
16 CH₃F at elevated temperatures. *Phys. Rev. A* **1998**, *57*, 4322-4326.
- 18 (53) Nagels, B.; Schuurman, M.; Chapovsky, P. L.; Hermans, L. J. F. Intermolecular versus
19 intramolecular interactions in nuclear spin conversion: Experiments on ¹³CH₃F–O₂. *J.*
20 *Chem. Phys.* **1995**, *103*, 5161-5163.
- 22 (54) Nagels, B.; Schuurman, M.; Chapovsky, P. L.; Hermans, L. J. F. Nuclear spin conversion
23 in molecules: Experiments on ¹³CH₃F support a mixing-of-states model. *Phys. Rev. A*
24 **1996**, *54*, 2050-2055.
- 26 (55) Michaut, X.; Vasserot, A.-M.; Abouaf-Marguin, L. Temperature and time effects on the
27 rovibrational structure of fundamentals of H₂O trapped in solid argon: hindered rotation
28 and RTC satellite. *Vib. Spectrosc.* **2004**, *34*, 83-93.
- 30 (56) Turgeon, P.-A.; Vermette, J.; Alexandrowicz, G.; Peperstraete, Y.; Philippe, L.; Bertin,
31 M.; Fillion, J.-H.; Michaut, X.; Ayotte, P. Confinement effects on the nuclear spin isomer
32 conversion of H₂O. *J. Phys. Chem. A* **2017**, *121*, 1571-1576.
- 34 (57) Henfrey, N. F.; Thrush, B. A. A high-resolution study of the ν_3 and $2\nu_8^0$ bands of
35 propyne. *J. Mol. Spectrosc.* **1987**, *121*, 150-166.
- 37 (58) Bode, J. H. G.; Smit, W. M. A.; Visser, T.; Verkruijsse, H. D. The absolute infrared
38 intensities of propyne-d₀ and propyne-d₃. *J. Chem. Phys.* **1980**, *72*, 6560-6570.
- 39 (59) Doney, K. D.; Zhao, D.; Bouwman, J.; Linnartz, H. The high-resolution infrared
40 spectrum of the $\nu_3+\nu_5$ combination band of jet-cooled propyne. *Chem. Phys. Lett.* **2017**,
41 *684*, 351-356.
- 43 (60) Duncan, J. L.; McKean, D. C.; Nivellini, G. D. The harmonic force field of methyl
44 acetylene. *J. Mol. Struct.* **1976**, *32*, 255-268.
- 46 (61) Anttila, R.; Sahlstro, T.; Jaakkone, S. Investigation of some vibration-rotation bands of
47 methyl acetylene in near-infrared. *Spectrochimica Acta* **1972**, *A28*, 1615-1623.
- 49 (62) Villa, M.; Fusina, L.; Nivellini, G.; Didriche, K.; de Ghellinck, X.; Vaernewijck, d. E.;
50 Herman, M. The infrared spectrum of propyne in the range 6200–6700 cm⁻¹. *Chem. Phys.*
51 **2012**, *402*, 14-21.
- 53 (63) Baylor, L. C.; Weitz, E.; Hofmann, P. Overtone spectroscopy of propyne and propyne-d₁.
54 *J. Chem. Phys.* **1989**, *90*, 615-627.
- 55
56
57
58
59
60

- 1
2
3 (64) Urban, S.; Pracna, P.; Graner, G. Ground state energy levels of propyne: Conventional
4 approach and Pade approximant. *J. Mol. Spectrosc.* **1995**, *169*, 185-189.
5
6
7
8
9
10
11
12
13
14
15
16
17
18
19
20
21
22
23
24
25
26
27
28
29
30
31
32
33
34
35
36
37
38
39
40
41
42
43
44
45
46
47
48
49
50
51
52
53
54
55
56
57
58
59
60

Table 1. Peak Positions and Widths (FWHM) in cm⁻¹ of Propyne (¹²C₃H₄) Trapped in Solid pH₂ at 1.7 K.

| Mode | NSI ^a | $\Delta K_{\nu}(K'')$ ^b | gas ^c | pH ₂ (FWHM) | Shift | Ref. |
|--|------------------|---|------------------|------------------------|--------|-------|
| 2v ₁₀ ⁰ (A ₁) | <i>o/p</i> | Q ₂ (0)/Q ₂ (1) | 650.352 | 665.44(0.82) | 15.09 | 42 |
| v ₅ (A ₁) | <i>o/p</i> | Q ₁ (0)/Q ₁ (1) | 930.277 | 929.81(0.13) | -0.46 | 42 |
| 2v ₉ ⁰ (A ₁) | <i>o/p</i> | Q ₂ (0)/Q ₂ (1) | 1254.347 | 1254.47(0.99) | 0.12 | 44 |
| v ₄ (A ₁) | <i>o/p</i> | Q ₁ (0)/Q ₁ (1) | 1385.579 | 1384.09(1.04) | -1.49 | 41 |
| 2v ₈ ⁰ (A ₁) | <i>o/p</i> | Q ₂ (0)/Q ₂ (1) | 2066.33 | 2058.65(0.50) | -7.68 | 57 |
| v ₃ (A ₁) | <i>o/p</i> | Q ₁ (0)/Q ₁ (1) | 2137.87 | 2138.34(0.04), m | 0.47 | 57 |
| (v ₃ +2v ₉) ⁺³ (A ₁) | <i>o/p</i> | Q _{1,2} (0)/Q _{1,2} (1) | 2336.95 | 2310.35(1.25) | -26.60 | 34 |
| v ₇ +v ₈ +v ₉ (A ₁) | <i>o/p</i> | Q _{1,1,1} (0)/Q _{1,1,1} (1) | 2760 | 2763.71(0.77) | -23.40 | 58 |
| 2v ₄ (A ₁)? | <i>o/p</i> | Q ₂ (0)/Q ₂ (1) | 2760 | 2751.99(3.65) | -8.01 | 58 |
| 2v ₇ ⁰ (A ₁) | <i>ortho</i> | Q ₂ (0) | 2879 | 2870.8(1.1), f | -7.8 | 34 |
| 2v ₇ ⁰ (A ₁) | <i>para</i> | Q ₂ (1) | | 2871.4(0.9), f | | |
| v ₂ (A ₁) | <i>o/p</i> | NR | | 2934.4, sh | | |
| v ₂ (A ₁) | <i>para</i> | Q ₁ (1) | 2940.944 | 2934.49(0.15), f | -6.46 | 35,45 |
| v ₂ (A ₁) | <i>ortho</i> | Q ₁ (0) | 2941.000 | 2934.60(0.16), f | -6.40 | 35,45 |
| v ₃ +v ₅ (A ₁) | <i>o/p</i> | NR | | 3065.7, sh | | |
| v ₃ +v ₅ (A ₁) | <i>para</i> | Q _{1,1} (1) | 3070.123 | 3066.01(0.04) | -4.11 | 59 |
| v ₃ +v ₅ (A ₁) | <i>ortho</i> | Q _{1,1} (0) | 3070.141 | 3066.14(0.30) | -4.00 | 59 |
| v ₁ (A ₁) | <i>o/p</i> | Q ₁ (0)/Q ₁ (1) | 3335.066 | 3328.52(0.07), m | -6.54 | 35 |
| v ₃ +2v ₉ ⁰ (A ₁) | <i>o/p</i> | Q _{1,2} (0)/Q _{1,2} (1) | 3381.15 | 3377.93(1.09) | -3.22 | 60 |
| 2v ₂ (A ₁) | <i>ortho</i> | Q ₂ (0) | 5781 | 5766.77(1.20), f | -14.23 | 37 |
| 2v ₂ (A ₁) | <i>para</i> | Q ₂ (1) | | 5769.10(1.11), f | | |
| v ₂ +2v ₇ ⁰ (A ₁) | <i>para</i> | Q _{1,2} (1) | | 5815.14(1.61), f | | |
| v ₂ +2v ₇ ⁰ (A ₁) | <i>ortho</i> | Q _{1,2} (0) | 5828 | 5814.72(0.99), f | -13.28 | 37 |
| 2v ₆ ⁰ (A ₁) | <i>para</i> | Q ₂ (1) | | 5906.14(0.89), f | | |
| 2v ₆ ⁰ (A ₁) | <i>ortho</i> | Q ₂ (0) | 5917.32 | 5906.40(0.85), f | -10.78 | 61 |
| v ₁ +v ₂ (A ₁) | <i>o/p</i> | Q _{1,1} (0)/Q _{1,1} (1) | 6275.841 | 6262.86(0.67) | -12.98 | 62 |
| v ₁ +v ₃ +v ₅ (A ₁) | <i>o/p</i> | Q _{1,1,1} (0)/Q _{1,1,1} (1) | 6399.463 | 6361.05(0.19) | -29.18 | 62 |
| 2v ₁ (A ₁) | <i>o/p</i> | Q ₂ (0)/Q ₂ (1) | 6567.878 | 6555.13(0.17), m | -12.75 | 62 |
| v ₁ +v ₃ +2v ₉ ⁰ (A ₁) | <i>o/p</i> | Q _{1,1,2} (0)/Q _{1,1,2} (1) | 6660.222 | 6652.00(2.11) | -8.22 | 62 |
| v ₉ (E) | <i>o/p</i> | $\tilde{\nu}_0$ /NR | 638.575 | 633.47(0.76) | -5.11 | 42 |
| v ₈ (E) | <i>para</i> | P ₁ (1) | 1030.554 | 1029.76(0.11) | -0.79 | 42 |
| v ₈ (E) | <i>o/p</i> | NR | | 1029.93(0.06) | | |
| v ₈ (E) | <i>o/p</i> | $\tilde{\nu}_0$ /NR | 1036.148 | 1031.30(0.17) | -4.85 | 42 |
| v ₈ (E) | <i>ortho</i> | R ₁ (0) | 1037.384 | 1034.8, sh | -2.58 | 42 |
| v ₈ (E) | <i>ortho</i> | R ₁ (0) | 1037.384 | 1035.05(0.22) | -2.34 | 42 |
| v ₇ (E) | <i>para</i> | P ₁ (1) | 1444.678 | 1443.54(0.45) | -1.14 | 41 |
| v ₇ (E) | <i>o/p</i> | NR | | 1444.93(0.46) | | |
| v ₇ (E) | <i>o/p</i> | $\tilde{\nu}_0$ /NR | 1450.271 | 1446.04(0.39) | -4.24 | |
| v ₇ (E) | <i>o/p</i> | NR | | 1451.46(0.61) | | |
| v ₇ (E) | <i>ortho</i> | R ₁ (0) | 1459.131 | 1454.67(0.12), sh | -4.46 | 41 |
| v ₇ (E) | <i>ortho</i> | R ₁ (0) | 1459.131 | 1455.12(1.06) | -4.01 | 41 |
| v ₇ (E) | <i>para</i> | R ₁ (1) | 1472.926 | 1473.88(4.60) | 0.96 | 41 |
| 2v ₇ ⁺² (E) | <i>para</i> | P ₂ (1) | | 2887.17(0.62) | | |
| 2v ₇ ⁺² (E) | <i>ortho</i> | R ₂ (0) | | 2890.08(0.86) | | |
| 2v ₇ ⁺² (E) | <i>para</i> | R ₂ (1) | | 2898.63(0.44) | | |
| v ₆ (E) | <i>para</i> | P ₁ (2) | 2965.400 | 2963.15(1.49) | -2.25 | 46 |
| v ₆ (E) | <i>para</i> | P ₁ (1) | 2975.259 | 2971.48(0.60) | -3.77 | 46 |

| | | | | | | | |
|----|-----------------------------|--------------|---------------------------|----------|---------------|--------|----|
| 1 | | | | | | | |
| 2 | | | | | | | |
| 3 | $\nu_6(E)$ | <i>o/p</i> | NR | | 2972.95(0.50) | | |
| 4 | $\nu_6(E)$ | <i>o/p</i> | $\tilde{\nu}_0/\text{NR}$ | 2980.852 | 2975.96(0.53) | -4.90 | 46 |
| 5 | $\nu_6(E)$ | <i>o/p</i> | NR | | 2978.29(0.24) | | |
| 6 | $\nu_6(E)$ | <i>ortho</i> | $R_1(0)$ | 2985.666 | 2979.00(0.46) | -6.67 | 46 |
| 7 | $\nu_6(E)$ | <i>ortho</i> | $R_1(0)$ | 2985.666 | 2980.37(0.46) | -5.30 | 46 |
| 8 | $\nu_6(E)$ | <i>para</i> | $R_1(1)$ | 2995.479 | 2984.93(1.60) | -10.55 | 46 |
| 9 | $\nu_6(E)$ | <i>para</i> | $R_1(1)$ | 2995.479 | 2985.5, sh | -9.98 | 46 |
| 10 | $\nu_6(E)$ | <i>para</i> | $R_1(2)$ | 3005.266 | 2997.19(4.32) | -8.07 | 46 |
| 11 | $\nu_3+\nu_8(E)$ | <i>para</i> | $P_{1,1}(1)$ | 3170.484 | 3165.99(0.13) | -4.49 | 47 |
| 12 | $\nu_3+\nu_8(E)$ | <i>o/p</i> | NR | | 3166.17(0.06) | | |
| 13 | $\nu_3+\nu_8(E)$ | <i>o/p</i> | $\tilde{\nu}_0/\text{NR}$ | 3176.077 | 3167.37(0.16) | -8.70 | 47 |
| 14 | $\nu_3+\nu_8(E)$ | <i>o/p</i> | NR | | 3170.90(0.13) | | |
| 15 | $\nu_3+\nu_8(E)$ | <i>ortho</i> | $R_{1,1}(0)$ | 3177.373 | 3171.31(0.20) | -6.07 | 47 |
| 16 | $\nu_3+\nu_8(E)$ | <i>para</i> | $R_{1,1}(1)$ | 3183.759 | 3175.82(0.31) | -7.94 | 47 |
| 17 | $\nu_1+\nu_9(E)$ | <i>para</i> | $P_{1,1}(1)$ | | 3956.55(50) | | |
| 18 | $\nu_1+\nu_9(E)$ | <i>o/p</i> | $\tilde{\nu}_0/\text{NR}$ | 3947.60 | 3957.97(0.32) | 10.37 | 63 |
| 19 | $\nu_1+\nu_9(E)$ | <i>ortho</i> | $R_{1,1}(0)$ | | 3962.04(0.94) | | |
| 20 | $\nu_1+\nu_9(E)$ | <i>para</i> | $R_{1,1}(1)$ | | 3965.97(0.52) | | |
| 21 | $\nu_2+\nu_6^{\pm 1}(E)$ | <i>o/p</i> | NR? | | 5780.17(1.49) | | |
| 22 | $\nu_2+\nu_6^{\pm 1}(E)$ | <i>para</i> | $P_{1,1}(1)$ | | 5784.68(0.18) | | |
| 23 | $\nu_2+\nu_6^{\pm 1}(E)$ | <i>o/p</i> | $\tilde{\nu}_0$ | 5790 | | | 37 |
| 24 | $\nu_2+\nu_6^{\pm 1}(E)$ | <i>ortho</i> | $R_{1,1}(0)$ | | 5789.85(7.48) | | |
| 25 | $\nu_6^{\pm 1}+2\nu_7^0(E)$ | <i>para</i> | $P_{1,2}(1)$ | | 5835.37(0.07) | | |
| 26 | $\nu_6^{\pm 1}+2\nu_7^0(E)$ | <i>o/p</i> | $\tilde{\nu}_0$ | 5852 | | | 37 |
| 27 | $\nu_6^{\pm 1}+2\nu_7^0(E)$ | <i>ortho</i> | $R_{1,2}(0)$ | | 5841.14(1.05) | | |
| 28 | $2\nu_6^{\pm 2}(E)$ | <i>para</i> | $P_2(1)$ | | 5938.42(0.75) | | |
| 29 | $2\nu_6^{\pm 2}(E)$ | <i>o/p</i> | NR | | 5939.62(0.42) | | |
| 30 | $2\nu_6^{\pm 2}(E)$ | <i>o/p</i> | $\tilde{\nu}_0/\text{NR}$ | 5953 | 5941.89(0.28) | -11.11 | 37 |
| 31 | $2\nu_6^{\pm 2}(E)$ | <i>o/p</i> | NR | | 5945.38(0.48) | | |
| 32 | $2\nu_6^{\pm 2}(E)$ | <i>ortho</i> | $R_2(0)$ | 5958 | 5947.05(0.82) | -10.95 | 63 |
| 33 | $2\nu_6^{\pm 2}(E)$ | <i>ortho</i> | $R_2(0)$ | 5958 | 5948.27(0.37) | -9.73 | 63 |
| 34 | $2\nu_6^{\pm 2}(E)$ | <i>para</i> | $R_2(1)$ | | 5792.66(0.46) | | |
| 35 | $\nu_1+\nu_6^{\pm 1}(E)$ | <i>para</i> | $P_{1,1}(1)$ | | 6284.58(0.03) | | |
| 36 | $\nu_1+\nu_6^{\pm 1}(E)$ | <i>o/p</i> | $\tilde{\nu}_0/\text{NR}$ | 6315.786 | 6286.61(0.15) | -29.18 | 62 |
| 37 | $\nu_1+\nu_6^{\pm 1}(E)$ | <i>ortho</i> | $R_{1,1}(0)$ | | 6288.82(0.14) | | |
| 38 | | | | | | | |
| 39 | | | | | | | |

^aNuclear Spin Isomer: *ortho* and *para* spin isomers; *o/p* indicates unresolved contributions. ^bNR stands for non-rotating; see text for details. ^cTaken from literature values or calculated using literature values and ground state spectroscopic constants of Ref. 64. f = value from fit; m = multiple peaks (principal peak listed), sh = shoulder.

Table 2. Parameters Determined from Observed Transition Frequencies and *POR*.

| Parameter | $\nu_6(E)$ | $\nu_7(E)$ | $\nu_3+\nu_8(E)$ | $\nu_6(E)$, <i>POR</i> |
|----------------------------------|----------------------|-----------------------|---------------------|-------------------------|
| $\tilde{\nu}_0 / \text{cm}^{-1}$ | 2976.59 | 1445.50 | 3170.53 | --- |
| A' / cm^{-1} | 3.62 | 5.77 | 4.13 | --- |
| ζ_i | 0.07250 ^a | -0.31424 ^a | 0.4052 ^a | --- |
| A'' / cm^{-1} | 5.10 | 1.96 | 4.54 | 2.22(55) |
| K'' values | 0, 1 | 0, 1 | 0, 1 | --- |

^a Fixed to gas-phase values: for ν_6 see Ref. 46, for ν_7 see Ref. 41, and for $\nu_3+\nu_8$ see Ref. 47.

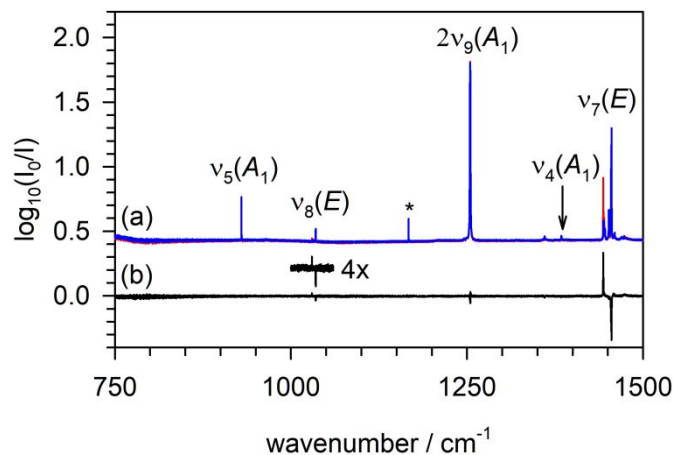


Figure 1. Infrared absorption spectra of propyne trapped in solid pD_2 at 1.70(1) K showing propyne absorptions in the 750-1500 cm^{-1} region. (a) Spectra recorded 2.63 (red) and 491 min (blue), respectively, after deposition of a 2.5(2) mm thick, 200(39) ppm propyne/ pD_2 sample. (b) Difference spectrum ($A_t - A_\infty$) calculated using the two spectra (before – after) displayed in trace (a) showing changes in peak intensities with time. The inset above (b) shows the difference signal multiplied by 4. The peak marked with * is the $U_0(0)$ transition of solid pD_2 . The $\nu_8(E)$ and $\nu_7(E)$ absorptions display peaks in the difference spectrum consistent with *para-to-ortho* NSC after deposition. See text for details.

(single column)

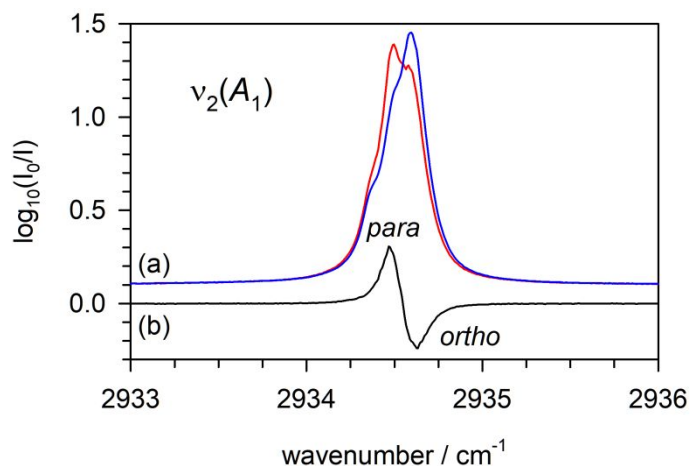


Figure 2. Infrared absorption spectra of propyne in solid pD_2 at 1.72(1) K in the region of the $\nu_2(A_1)$ fundamental. (a) Spectra recorded 5.08 (red) and 291.8 min (blue), respectively, after deposition of the sample shown in Figure 1. (b) Difference spectrum ($A_t - A_\infty$) calculated using the two spectra displayed in trace (a) showing changes in absorption intensity with time after deposition. The positive and negative peaks are labeled *para* and *ortho*, respectively, indicating the nuclear spin symmetry in the ground vibrational state associated with each peak. See text for details.

(single column)

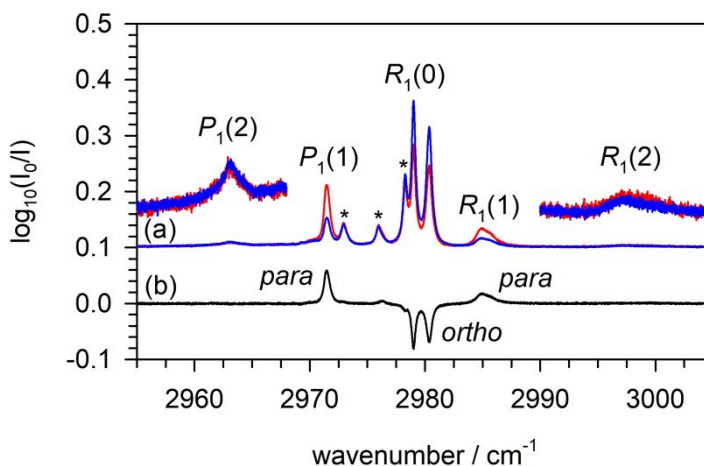


Figure 3. Infrared absorption spectra of propyne in solid pD_2 at 1.72(1) K in the region of the $\nu_6(E)$ fundamental. (a) Spectra recorded 5.08 (red) and 291.8 min (blue), respectively, after deposition of the sample shown in Figure 1. (b) Difference spectrum ($A_t - A_\infty$) calculated using the two spectra displayed in trace (a) showing how the absorption intensity changes with time after deposition. The positive and negative peaks are labeled *para* and *ortho*, respectively, indicating the nuclear spin symmetry in the ground vibrational state associated with each peak. Peaks marked with an asterisk do not show up in the difference spectrum. See text for details.

(single column)

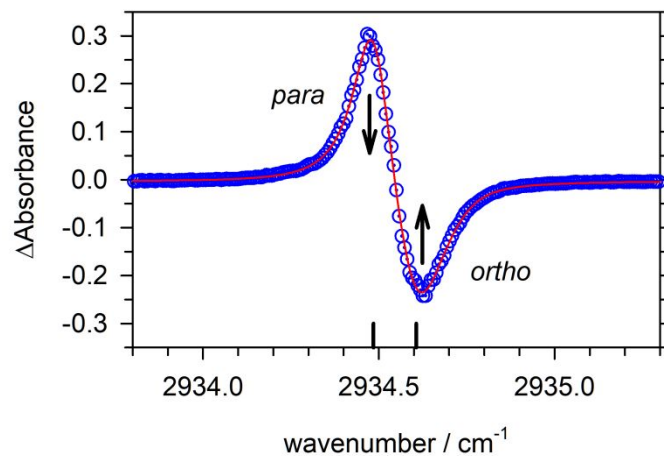


Figure 4. Fits of the ν_2 difference spectrum of propyne in solid $p\text{H}_2$ calculated using spectra recorded 5.08 and 291.8 min after deposition of the sample shown in Figure 1. The data are the blue circles and the results of a least squares fit to an analytic function is shown as a red line. The two black lines represent the average peak positions determined from fits to all the spectra for this kinetic run.

(single column)

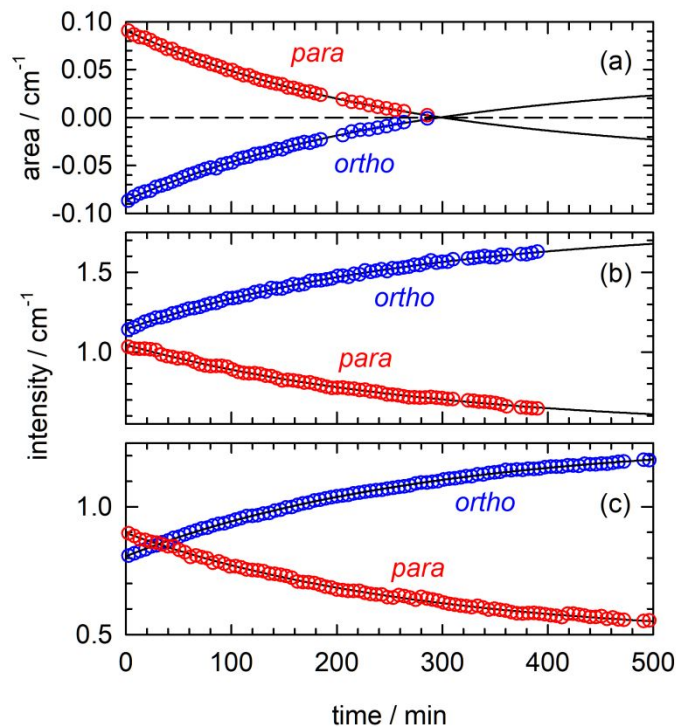


Figure 5. Representative kinetic traces of propyne NSC for propyne isolated in solid pH_2 at 1.7 K. (a) The red and blue data points correspond to the areas of the *para* and *ortho* peaks in the ν_2 difference spectrum of propyne for the sample shown in Figure 1. Integrated intensities of the *ortho* and *para* peaks assigned to (b) ν_6 and (c) ν_7 absorption bands for samples containing 289(16) and 200(39) ppm of propyne, respectively. The red and blue data points in (b) and (c) correspond to the integrated intensities of the *para* and *ortho* peaks.

(single column)

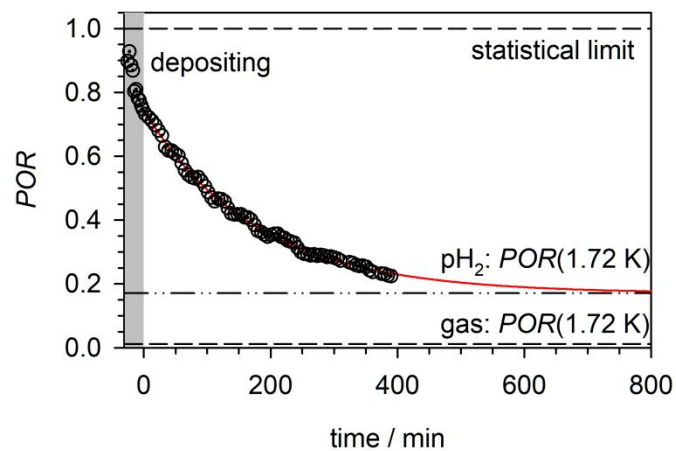


Figure 6. Representative kinetic trace (data shown in Fig. 5b) of the propyne *para-to-ortho* ratio (*POR*) measured as a function of time after deposition for propyne isolated in solid pH_2 at 1.7 K.

(single column)

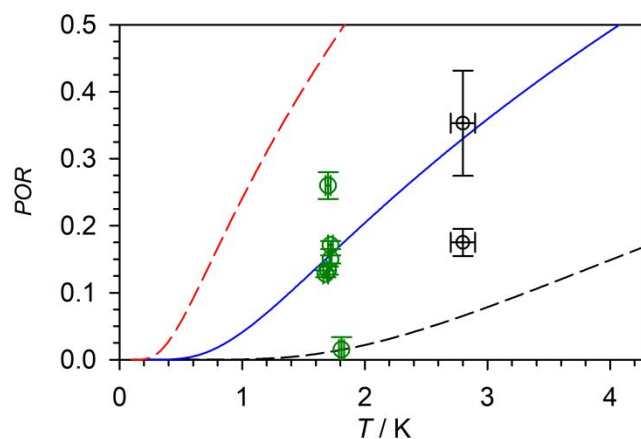


Figure 7. Plot of the equilibrium *POR* versus temperature (K) measured in this study. Data from samples grown in Wyoming and Orsay are plotted as green and black circles, respectively. The lines represent theoretical *POR* curves calculated for single-axis *K*-rotation with effective *A*'' constants equal to 1.00 cm⁻¹ (red dashed line), 2.22 cm⁻¹ (blue line), and 5.31 cm⁻¹ (black dashed line). All the measured values lie between the two limiting cases and are best represented by *A*''=2.22 cm⁻¹. See text and [Supporting Information](#), Tables S6 and S7 for more details.